Karazin Kharkiv National University

Department of Physics and Technology

Gesellschaft für Schwerionenforschung

mbH Darmstadt

GSI

Simulation of the magnetic field distribution in a toroidal magnetic flux concentrator

Diploma Thesis

Natalya Miski-Oglu

Darmstadt 2004

Abstract.

The present diploma thesis demonstrates the possibility of creating a new type of dc-current device – the magnetic flux concentrator. This device will monitor the increased beam intensities at the future GSI facility.

The accuracy of the measurements of the increased beam intensities using a magnetic flux concentrator is calculated. A key element is the use of numerical simulations to prove the proposed dc-current monitoring device's insensitivity to the variation of the beam position. The diploma thesis provides also an overview of the modern magnetic field sensors.

Анотація.

У даній дипломній роботі продемонстрована можливість збудування нового вимірювального пристрою для вимірювання строму пучків заряджених частинок - концентратора силових ліній магнітного поля. Цій пристрій буде використано для вимірювання строму пучків заряджених частинок у майбутньому циклічному прискорювачу заряджених частинок у лабораторії GSI (місто Дармштадт, Німеччина).

Головною метою дипломної роботі було показати, що варіації позиції пучка заряджених частинок не веде до зміни показань пристрою. Ця мета була досягнута за допомогою численних рахувань. У роботі також зроблено огляд нових засобів вимірювання магнітного поля.

Contents

1. Introduction.

The future GSI facility [1] will consist of a 100/200 Tm double-ring synchrotron SIS100/200 and a system of associated storage rings for beam collection, cooling, phase space optimization and experimentation. It uses the present accelerators, a universal linear accelerator (UNILAC) and a synchrotron ring accelerator (SIS18), as injector. The heart of the new facility, the double-ring synchrotron, provides for the fast acceleration utilizing novel, rapidly cycling superconducting magnets, which are presently under development in collaboration with laboratories in the USA and in Russia. A key feature of the new facility will be the generation of intense, high-quality secondary beams. These include beams of short-lived (radioactive) nuclei and beams of antiprotons. Secondary beams are produced in nuclear reactions induced by beams of stable particles. To achieve the desired intense secondary beams, the primary beam intensities must be correspondingly high. Compared to the present GSI facility, beam intensities in the proposed facility will be increased by a factor of 100 in primary beam intensities, and up to a factor of 10000 in secondary radioactive beam intensities. This increase in beam intensity is a key technical goal of the future GSI facility. To achieve this goal, it is necessary to solve several technical problems. In particularly, methods and devices for the monitoring of these intensely increased beam currents must be developed.

Chapter two presents the overview of two methods of beam current measurements: the beam transformer for pulsed beams and the dc-transformer, which is the monitoring device now being used at the GSI SIS18 facility.

The third chapter discusses the magnetic flux concentrator, including the choice of the yoke materials and the choice of the magnetic sensor.

The fourth chapter of this diploma work demonstrates the possibility of creating a new type of dc-current device that will monitor the increased beam intensities at the future GSI facility. In this chapter the accuracy of the measurements of the increased beam intensities using a magnetic flux

concentrator is calculated. A key element is the use of numerical simulations to prove the proposed dc-current monitoring device's insensitivity to changes in the beam position.

The fifth chapter discusses the results of the numerical simulations.

2. Methods of beam current measurements.

For the daily operation of any type of accelerator as well as for the storage rings, the main parameter is the current of charged particle beams. In most cases the beam current is measured with beam transformers. These devices are applicable for measuring ac beams in electron and proton pulsed LINACs, synchrotrons, and for measuring dc beams as in a storage ring. The working principle of a beam transformer is to detect the magnetic field aligned with the beam of charged particles. However, for low currents, the beam transformers will not work because of their noise floor. For low currents, particle detectors are used. In this case, the energy loss of the charged particle traveling through

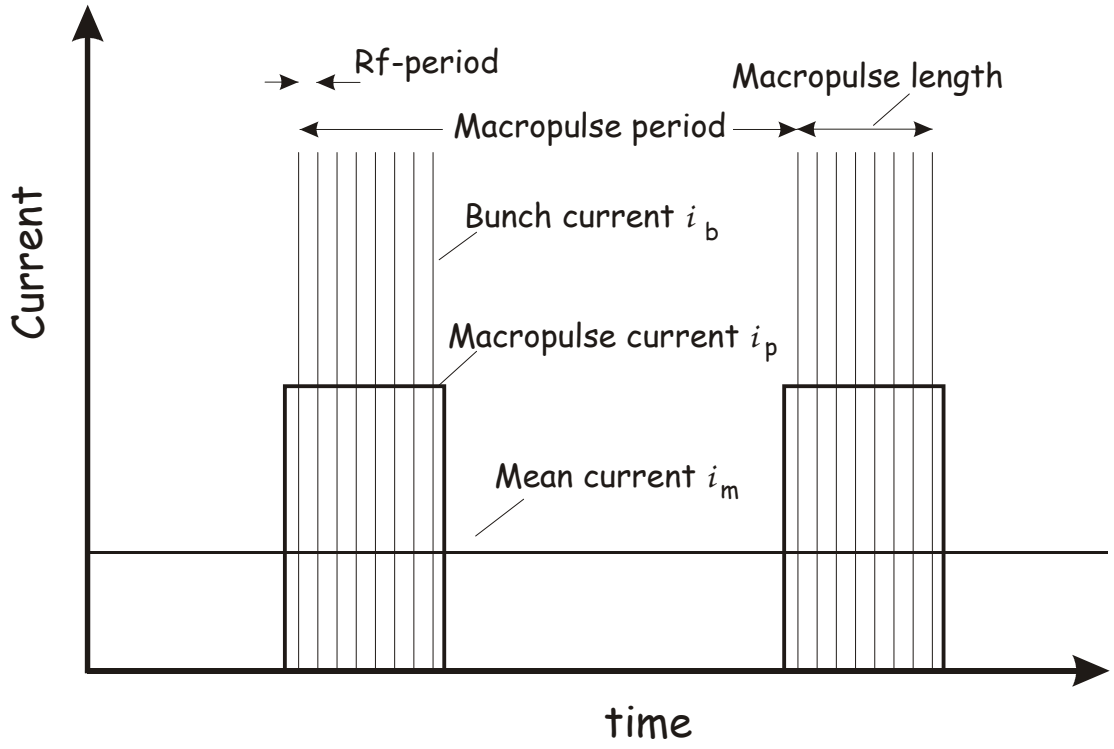

Fig. 2.1. The time structure of the beam current for a pulsed LINAC.

matter is detected. Another method for both low currents and moderate beams is to stop the particles in a Faraday cup in order to collect their charge. For high currents this destructive method cannot be applied, because the total energy carried by the beam will destroy the intersecting material. For high energetic particles the range reaches more than several cm and Faraday cups can no longer be used.

It is now necessary to describe the time structure of a current that must be detected. Figure 2.1 shows the time structure of a beam for the pulsed LINAC.

- The current within a bunch i_b is sometimes called the micropulse current.
- The macropulse current i_p is averaged over all micropulses within the macropulse length.
- The mean current i_m is averaged over many macropulse currents.

In the synchrotron accelerator the time structure of the beam differs from a pulsed LINAC. Here, the macropulse has an infinite length and the average current i_m is equal to the macropulse current i_p. The bunch structure still remains for rf accelerators.

In any accelerator the current is formed by N particles of charge state q per unit of time t or unit of length l and relative velocity $\beta = \frac{\mathrm{v}}{c}$. The electrical current is

$$I = \frac{q \cdot e \cdot N}{t} = \frac{q \cdot e \cdot N}{l} \beta c . \qquad (2.1)$$

The magnetic field $\vec{B}$ of a current can be calculated according to the Biot-Savart law

$$d\vec{B} = \mu_0 I \cdot \frac{d\vec{l} \times \vec{r}}{4\pi r^3}, \qquad (2.2)$$

where $\mu_0 = 1.26 \cdot 10^{-6}$ newton per square ampere (N / A^2) is the permeability of the vacuum, $d\vec{l}$ the infinitesimal vector in the direction of the current, and $\vec{r}$ is the distance between the current and the point where the field is measured. The magnetic field of an infinitely long linear current has only the azimuthal component. The absolute value is given by the formula 2.3 as

$$B = \mu_0 \frac{I}{2\pi r} . \qquad (2.3)$$

2.1. The beam transformer for pulsed beams.

The scheme of a “common” pulse transformer is shown in Figure 2.2. The alternating primary current flows through the primary winding with the coil

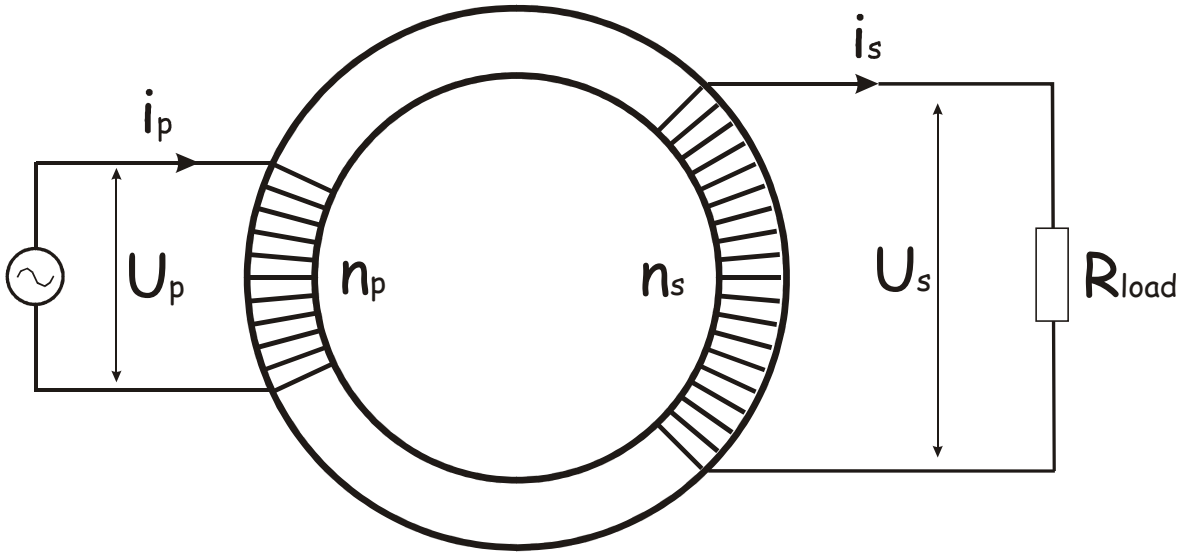

Fig. 2.2. The pulse transformer.

number n_p and produces changing magnetic flux in the magnetic yoke. The changing magnetic flux induces a voltage in each coil of the primary winding. This voltage is given by Faraday's law (2.4)

$$U_{ind} = -\frac{d\Phi}{dt}. \qquad (2.4)$$

The whole voltage across the prime winding is given by

$$U_w = n_p \cdot U_{ind}. \qquad (2.5)$$

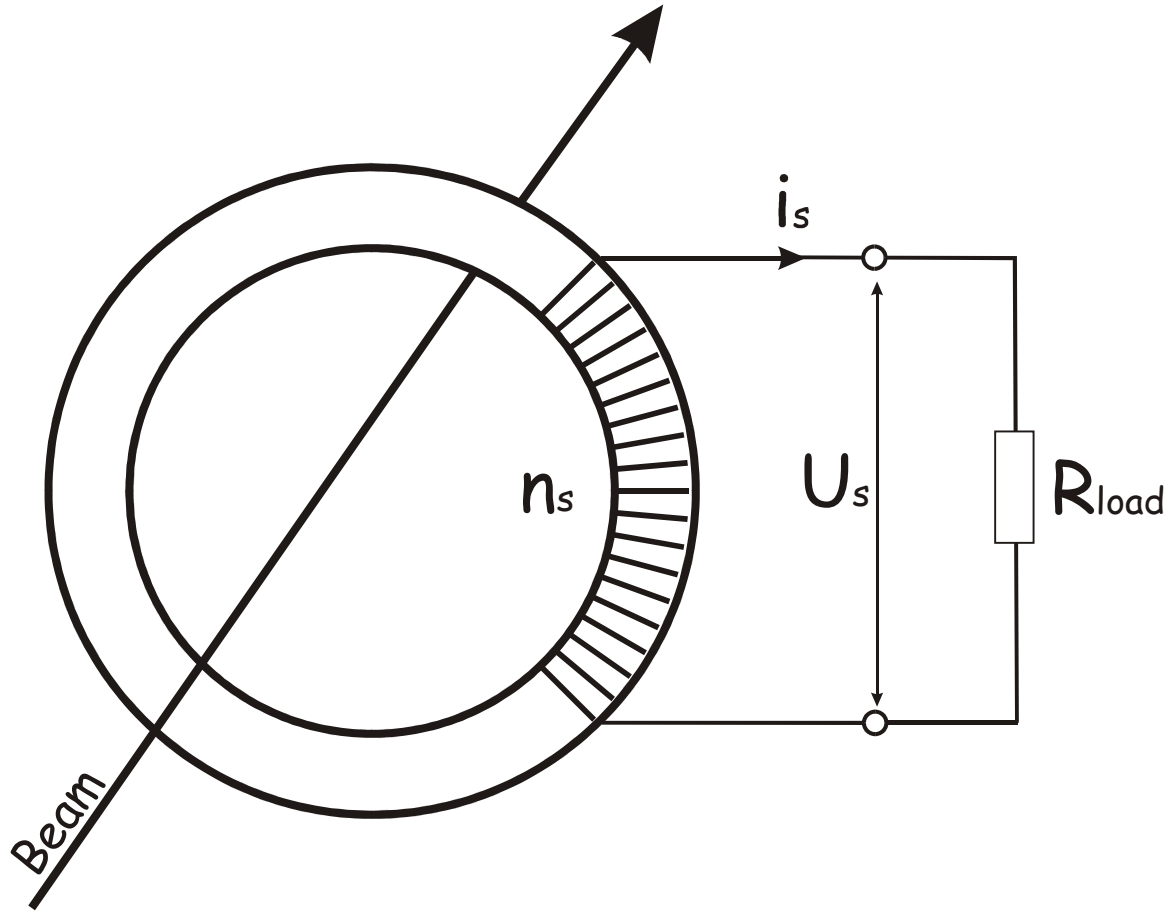

Fig. 2.3. The beam transformer.

The voltage source and inductance of the primary winding forms a closed circuit. In agreement with the second Kirchhoff's law, the sum of the voltage sources in a closed circuit is equal to zero. Thus $U_p + U_w = 0$ and

$$U_p = -n_p \cdot U_{ind} = n_p \cdot \frac{d\Phi}{dt}. \qquad (2.6)$$

For the ideal transformer the magnetic flux is the same for the secondary winding, with the coil number n_s. The alternating magnetic flux induces in the secondary winding a voltage (2.7)

$$U_s = -n_s \cdot \frac{d\Phi}{dt}. \qquad (2.7)$$

From the expressions (2.6) and (2.7) it follows that the voltage ratio between primary and secondary windings is

$$\frac{U_p}{U_s} = -\frac{n_p}{n_s}. \qquad (2.8)$$

In the case of an ideal transformer one can write

$$U_p \cdot i_p = U_s \cdot i_s. \qquad (2.9)$$

This gives immediately the current transformation ratio

$$\frac{i_p}{i_s} = -\frac{n_s}{n_p}. \qquad (2.10)$$

The beam transformer is the same as a current transformer, but with a reduced number of coils in the primary winding n_p, which is equal to one. Figure 2.3 illustrates a beam transformer. The beam is the primary winding. All formulas obtained for a current transformer are also applicable to a beam transformer.

For an understanding of the electromagnetic processes in a beam transformer, consider the following simplified model: the beam is a signal generator with an infinitely small inner resistance. The inductance of the first winding is formed by passing a beam through the aperture of the magnetic yoke.

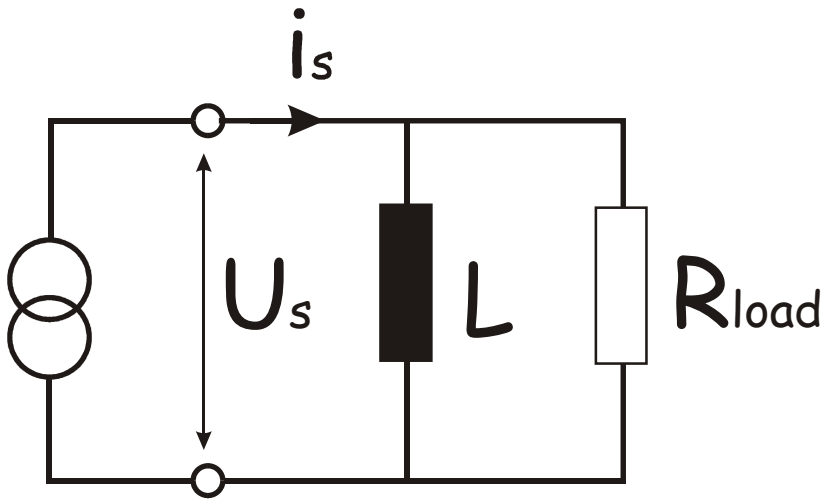

Fig. 2.4. The electrical equivalent scheme of the beam transformer. The inductance L represents the inductance of the secondary winding. The ideal current source represents the induced current in the secondary winding.

The fact that the primary winding has only one coil lets us assume that the inductance of the primary windings is much smaller than the inductance of the secondary windings. This assumption allows us to suggest that the time dependence of the magnetic flux circuit linking the secondary winding is the same as that of the beam current. Whereas in a “common” pulse transformer, the presence of the first winding inductance causes a change in the magnetic flux. The electrical equivalent scheme corresponding to the above model is represented in Figure 2.4.

In agreement with Ohm’s law the secondary current is $i_s = i_l + i_R$, the current through inductance is

$$i_L(t) = \frac{1}{L} \cdot \int_0^t U_s(t)dt \ . \qquad (2.11)$$

The Ohm’s law, together with the last expression, gives the equation for U_s

$$i_s(t) = \frac{1}{L} \cdot \int_0^t U_s(t)dt + \frac{U_s(t)}{R_{load}} \ . \qquad (2.12)$$

The differentiation of the last expression gives the differential equation (2.13) for an unknown function U_s with given function i_s

$$\frac{1}{R} \cdot \frac{dU_s}{dt} + \frac{1}{L} \cdot U_s = \frac{di_s}{dt} . \qquad (2.13)$$

It is important to know how the voltage U_s behaves when the current i_s changes like a staircase function

$$i_s = \begin{cases} 0 & for \quad t < 0 \\ & \\ I_0 & for \quad t \geq 0 \end{cases} , \qquad (2.14)$$

where $I_0 = \frac{I_{beam}}{n_s}$. The solution of equation 2.13 with function 2.14 and the initial condition $U(0) = I_0 \cdot R_{load}$ is

$$U_s(t) = \frac{I_{beam}}{n_s} R_{load} \cdot e^{-\frac{t}{\tau}} \quad , \qquad (2.15)$$

where $\tau = \frac{L}{R_{load}}$ is the drop time. From this result it is clear that for the registration of the beam pulse with length t_{pulse}, the τ must be much bigger than t_{pulse}. Thus, for registration of long pulses, the inductance L must be large and the resistance of the load must be small. The last condition is realized when the ac-transformer is loaded by the current-voltage transducer. In this case, a drop time of several seconds can be achieved. However, this will not allow to measure dc current. Thus, one of the possibilities is to directly measure the magnetic field of the dc current.

2.2. The dc-transformer.

The dc-transformer principle [2] is shown schematically in Figure 2.5. It consists of two cores with three windings each. The beam passes through the aperture of both cores. The primary windings with opposite orientation are used as a modulator. The modulation frequency is typical 0.1-1kHz. The amplitude of

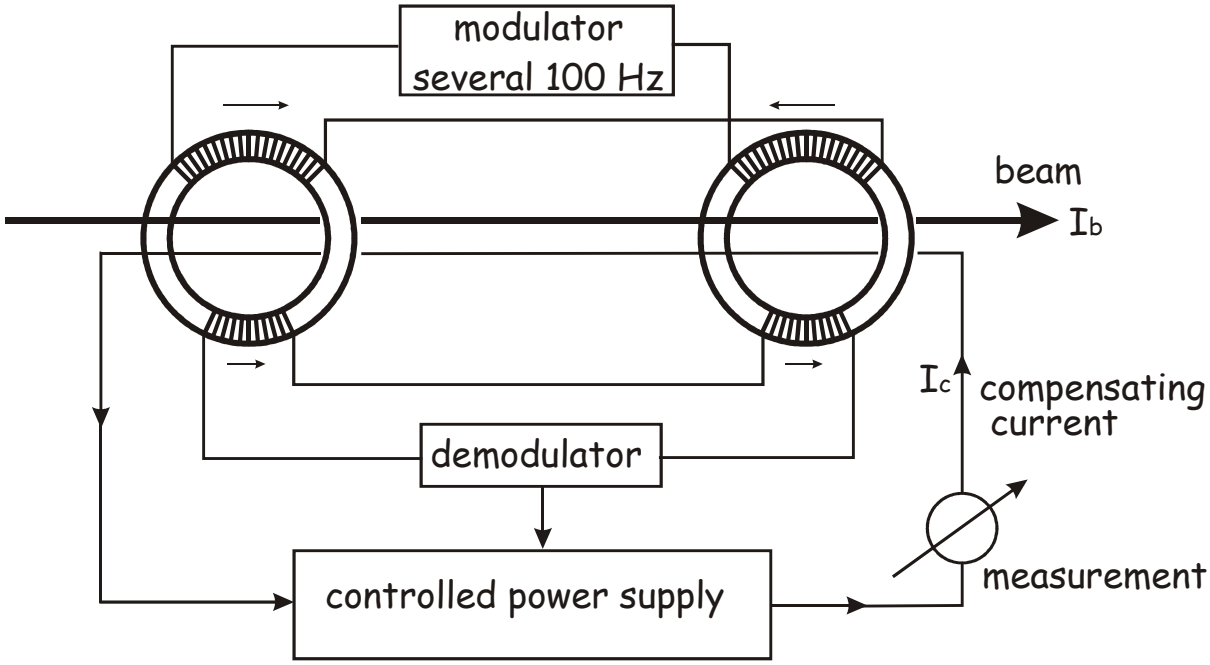

Fig. 2.5. Schematics of the dc-transformer.

the modulation current is strong enough to force the magnetization of the core into saturation, two times for each period. The secondary windings with equal orientation act as a detector for the modulated signal.

For simplicity, consider the modulating current having a triangular form. First of all look at the processes in the dc-transformer as in the example in Figure 2.6, which has no external magnetic field.

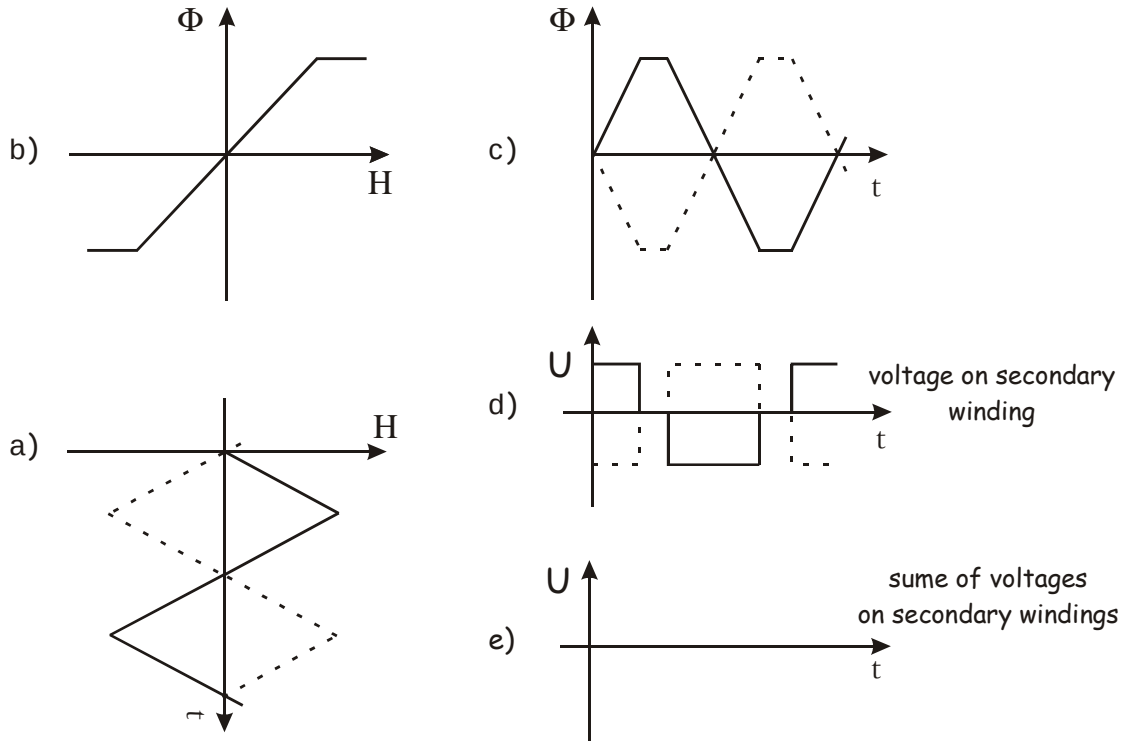

Fig. 2.6. The workings of the dc-transformer in the absence of an external magnetic field. Diagram **a** shows the modulation field, **b** shows the flux-field dependence, **c** shows the resulting change of the flux, **d** and **e** show the induced voltage in the secondary windings.

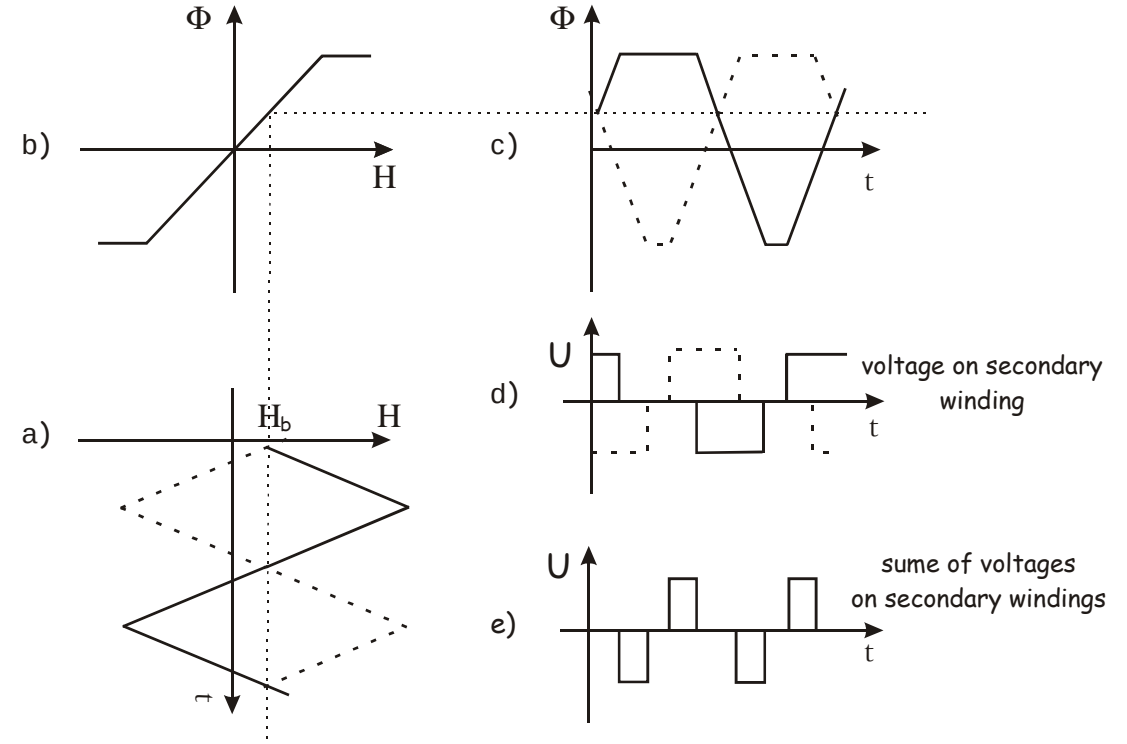

Fig. 2.7. The workings of the dc-transformer in the presence of an external magnetic field H_b. Diagram **a** shows the modulation field, **b** shows the flux-field dependence, **c** shows the resulting change of the flux, **d** and **e** show the induced voltage in the secondary windings.

The modulating current produces the magnetic field H. The time dependence of magnetic field H is presented in Figure 2.6.a. This field forces the core material to become saturated. All of the curves drawn with a continuous line present the processes in one core, with the dotted line presenting the processes in the other core. The dependence between the flux of the magnetic induction and the magnetic field is non-linear. The field-flux dependence is shown by the curve in Figure 2.6.b. The flux of the magnetic induction has a time dependence as shown in Figure 2.6.c. Notice that the flux time dependence curve has a trapezium form because the core material has been saturated. In the absence of an external magnetic field, the area under the positive part of the flux curve is equal to the area under the negative part of the flux curve. In agreement with Faraday's law, the alternating flux induces a voltage in the secondary winding, which is proportional to the time derivative of the magnetic flux as shown in Figure 2.6.d. When the external magnetic field is zero, the voltage on each of the two secondary windings is identical up to a phase shift of 180 degres. The algebraic sum of these two voltages is equal to zero.

Now consider the processes in the dc-transformer in the presence of an external magnetic field. Figure 2.7.a shows the curve which represents the time dependence of the magnetic field. Notice that this curve is shifted on the basis of the value of the external magnetic field H_b. Now, the area under the positive part of the curve is no longer equal to the area under the negative part of the curve. The curve in Figure 2.7.c represents the time dependence of the flux. The area under the positive part of this curve is no longer equal to the area under the negative part of the curve. The voltage on the secondary windings have a phase shift which is not equal to 180 degrees. The algebraic sum of the secondary voltages is no longer equal to zero, but is now proportional to the external magnetic field. In the demodulator stage represented in Figure 2.5, this signal is rectified. The magnetic field is measured by means of the feedback current which is generated in the automatic compensation circuit. The feedback current

forces the sum of the secondary voltage to zero again. This feedback current flows through the compensating windings. In Figure 2.5 these windings are shown as lines parallel to the beam. The feedback circuit for the zero flux compensation makes the device very sensitive and linear. To get a faster response, the signal from the ac-transformer is added to the dc-feedback circuit.

The devices based on this principle are used in many accelerator laboratories, particularly at the GSI heavy ion synchrotron SIS18. To achieve high resolution and time stability of the dc-transformer a core pair with identical magnetic characteristics is needed. It is very difficult to produce a core pair with identical magnetic characteristics. The design of a dc-transformer with high resolution and time stability is rather complex and its success depends very much on the selection and treatment of the core material as discussed more in detail in [3]. The above specified problem makes this device expensive and the production of numbers of such devices is a difficult problem.

3. The magnetic flux concentrator.

At present, the only device being used to measure a continuous beam current is the dc-current transformer. However, a new idea for measuring a

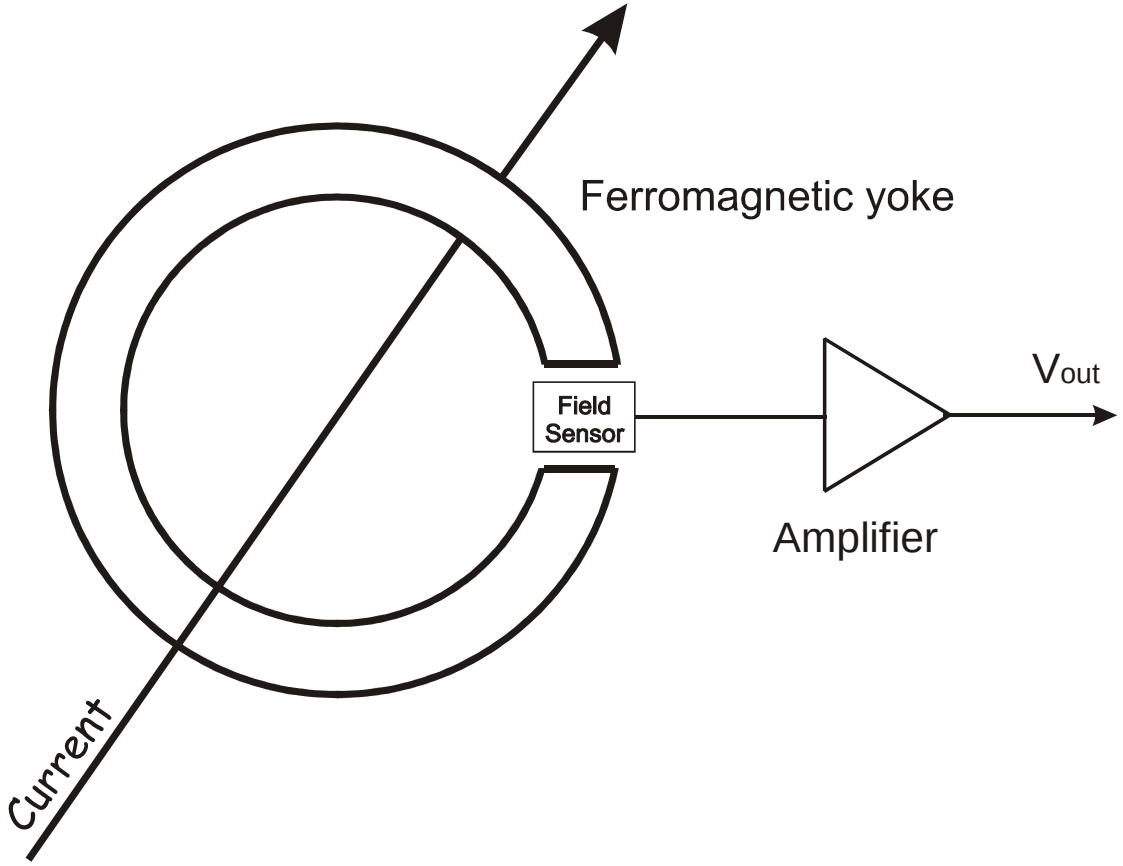

Fig. 3.1. The open loop current sensor.

continuous beam current has been proposed: the use of a magnetic flux concentrator.

The operation of a magnetic flux concentrator is very simple. It is illustrated in Figure 3.1. A beam current is passed through the aperture of the magnetic yoke and produces a magnetic field proportional to the current magnitude. The yoke concentrates the magnetic field around a Hall sensor that has been placed in the air gap. The output of the magnetic field sensor is fed into an amplifier. The output voltage of the amplifier is proportional to the current that is passed through the aperture of the magnetic yoke.

The type of the measured current can be either AC or DC.

The combination of well known magnetic materials, such as VITROVAC, with the recently developed magnetic field sensors that are based on the AMR (Anisotropic Magnetoresistivity) effect, or the GMR (Giant Magnetoresistivity) effect, can lead to the creation of a new, very precise and easily reproduced device for measuring beam currents.

The linearity and frequency properties of such devices are determined by the characteristics of the magnetic yoke and the magnetic field sensor. Both the magnetic yoke and the magnetic field sensor are non-linear in a strong magnetic field. Thus such a construction has restrictions on the magnitude of the measuring current.

To avoid the difficulties with the linearity one can use the feedback signal from the current sensor. Figure 3.2 illustrates the principle of the magnetic flux

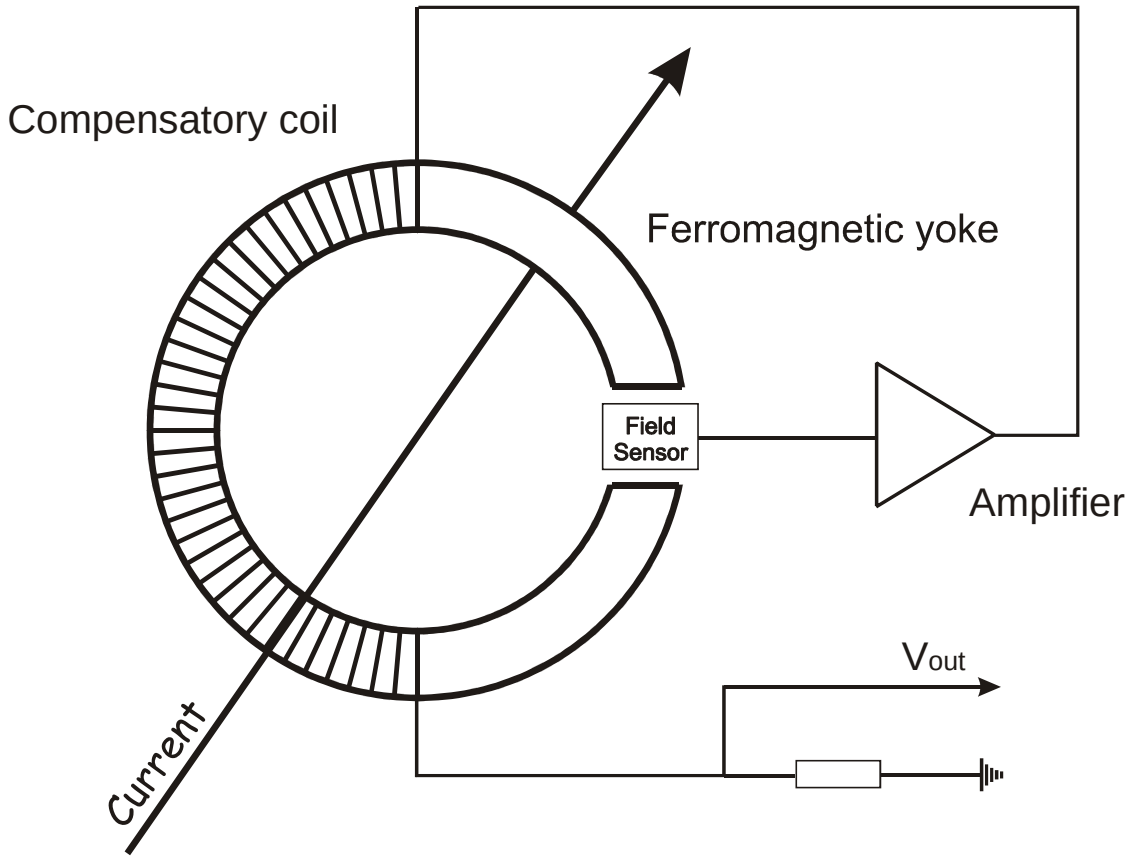

Fig. 3.2. The closed loop current sensor.

concentrator with an applied feedback loop. A beam current passes through the

aperture of the magnetic yoke and produces a magnetic field proportional to the current. The yoke concentrates the magnetic field around e.g. a Hall sensor that is placed in the air gap. The output of the magnetic field sensor is fed into an amplifier. The output voltage of the amplifier is proportional to the current that passes through the aperture of the magnetic yoke. The output of the amplifier is fed into a push-pull driver stage that drives a compensatory coil that is wound around the magnetic yoke. The coil produces a magnetic field that is equal, but opposite to that of the sensing current. Thus, the magnetic flux in the magnetic yoke – for all values of the measuring current – is still near to zero. Therefore, the magnetic yoke and the Hall sensor always stay in the linear mode of operation.

The main parts of the future GSI facility are synchrotron SIS100/200. These will provide ion beams with a very high current of up to 100 A. The device will be designed to measure a beam current of up to 100 A. The lower limit must be as low as possible. One (1) mA was chosen as the lower limit. These parameters are mainly defined by the properties of the magnetic field sensors.

The requirements for the time resolution – otherwise known as the bandwidth – is defined by the duration of the injection, the acceleration, the various manipulations of the beam time structure, and, of course, by the beam extraction. The duration of these processes lie within a very wide time region, from several seconds down 25 nanoseconds. The required bandwidth is 10MHz or more. The bandwidth of the whole device depends on eddy current losses in the yoke material and on the bandwidth of the magnetic sensor.

3.1. The choice of the yoke material.

In order to provide the largest gain for the detected magnetic field, the material from which the yoke is constructed must have a magnetic permeability value as high as possible. One of the possible yoke material candidates is the material VITROVAC 6025f, manufactured by the company ”Vacuumschmelze AG”. This material is an amorphous alloy $(CoFe)_{70\%}(MoSiB)_{30\%}$ manufactured using a special magnetic annealing procedure. VITROVAC 6025f has a pulse permeability of about 100000 which is a hundred times larger than other comparable magnetic materials [4]. Figure 3.3 shows the field-flux curve which

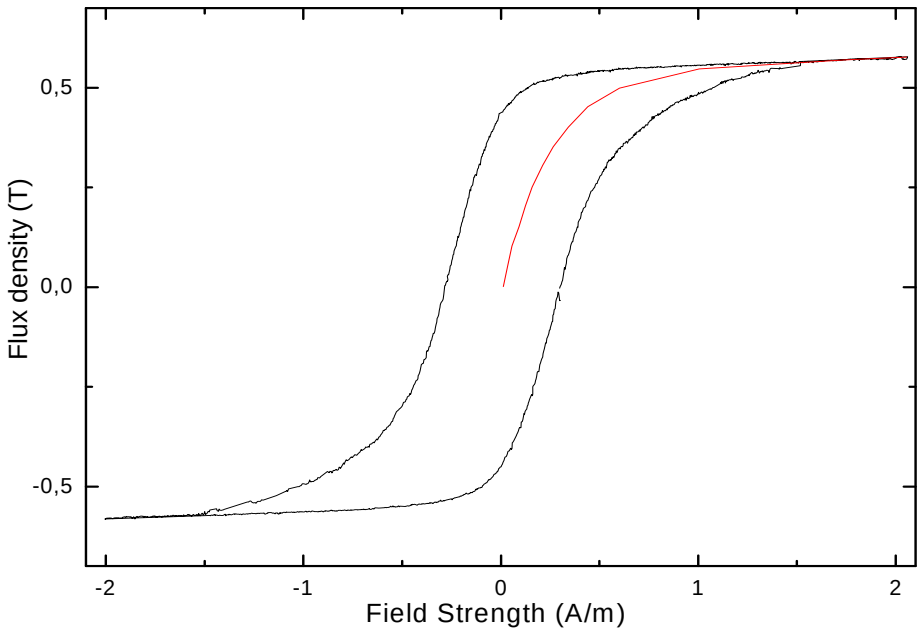

Fig. 3.3. The hystereses curve for magnetic material VITROVAC 6025f.

was measured at GSI during their development of ac and dc-transformers.

In [4], VITROVAC 6025f is recommended as the material to be used for signal transformers. VITROVAC 6025f has an extremely smooth insertion loss curve, without dips in resonances of up to 30 MHz. This fact, and the experience gained during the creation and operation of the ac- and dc-transformers, suggest that, with VITROVAC 6025f used as the yoke material, it is possible to achieve wide bandwidth for the magnetic flux concentrator.

3.2. The choice of the magnetic sensor.

Today, the technically most important sensors for magnetic fields measurements are:

- The Fluxmeter Method
- Hall sensors
- AMR (Anisotropic MagnetoResistive) sensors
- GMR (Giant MagnetoResistive) sensors
- SQUIDs (Superconducting Quantum Interference Devices).

The fluxmeter method is the oldest of the currently used methods for magnetic field measurements. The change of flux in a measurement coil induces a voltage across the coil's terminals. Measurements are performed either by using fixed coils in a dynamic magnetic field or by moving the coils in a static magnet field [5]. This method is very precise but the presence of moving parts required for static field measurements makes this method unsuitable for the measurement of the magnetic field in the air gap of a magnetic flux concentrator.

SQUID, the modern and most precise method of the magnetic field measurements, allows the detection of extremely low magnetic fields of about 5 fT. Because of its high costs and the need for liquid Helium temperature, this method is also unsuitable for the measurement of the magnetic field in the air gap of a magnetic flux concentrator.

Hall, AMR, and GMR sensors can be considered as possible sensor candidates for the magnetic flux concentrator (because of their low costs, small size, high sensitivity, and precision). A more detailed discussion of the way in which these sensors work and their possible utilization as a measurement tool follows.

3.2.1. The Hall sensor.

A particle with a charge Q, velocity $\vec{v}$ and moving within a magnetic field $\vec{B}$, will experience the Lorenz force,

$$\vec{F} = q \cdot (\vec{v} \times \vec{B}). \qquad (3.1)$$

The force direction is mutually perpendicular to the direction of the particle velocity and the magnetic field. If a long, flat current-carrying conductor is placed in a magnetic field, the moving charges will experience a net force mutually perpendicular to the direction of the current flow (longitudinal conductor axis) and the magnetic field. Under the influence of this force, the electrons will bend at one edge of the conductor, and positive charges will gather at the other edge. A lateral charge distribution results and gives rise to an electric field, $\vec{E}$, which exerts a force,

$$\vec{F} = q \cdot \vec{E}, \qquad (3.2)$$

in a direction opposite to the Lorenz force. At equilibrium, the resultant forces balance. This electrical field yields the potential difference U_{Hall} (3.3) between opposite sides parallel to the long axis of the conductor.

$$U_{Hall} = R \cdot I \cdot B, \qquad (3.3)$$

where R is a Hall constant obtained from a property of the material, B is a component of the magnetic field that is perpendicular to the surface of the conductor and current direction, and I is an electrical current that flows through the conductor. Figure 3.4 explains the manner by which the Hall sensor works.

The Hall constant is very small for metals and only sensors manufactured from InAs or GaAs semiconductor material have appropriate sensitivity. Typically, the sensitivity of Hall sensors is about 1V/($A_{\text{Hall current}} \cdot T_{\text{flux}}$) [6].

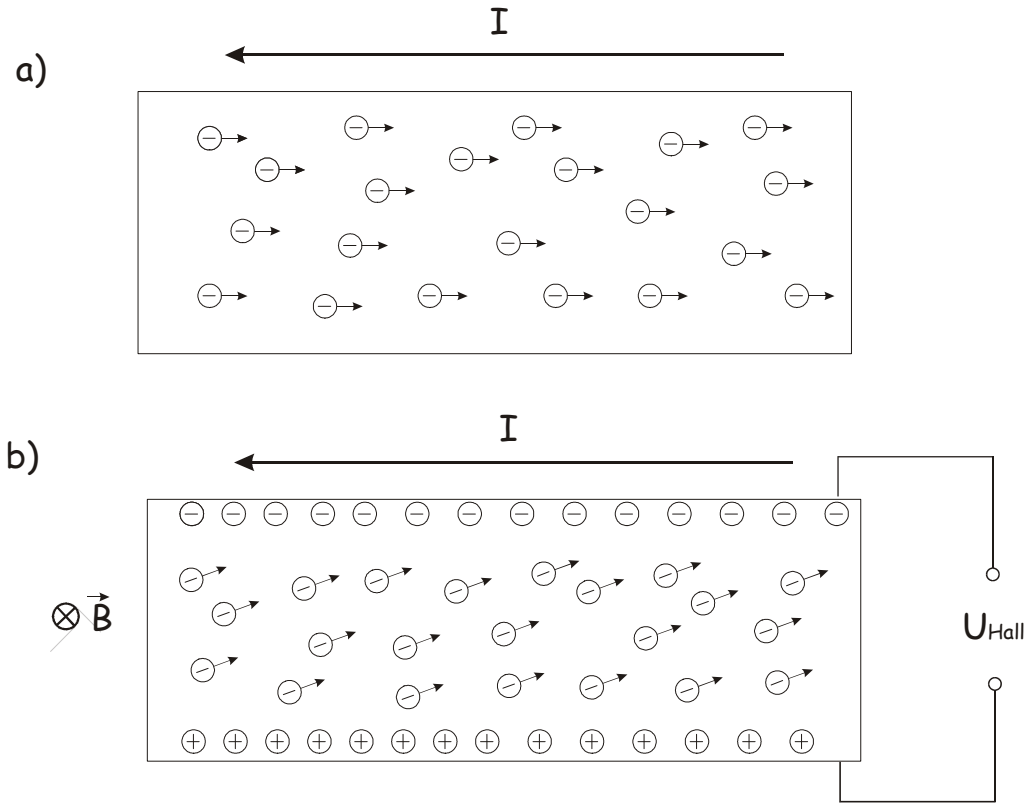

Fig. 3.4. The principle of the Hall effect. The figure a) shows the electrons movement in a flat current-carrying conductor without applied magnetic field. The figure b) shows the electrons movement in a flat current-carrying conductor with applied magnetic field.

In recent times, with improvements in the technology of thin ferromagnetic films, the number of commercially available Hall sensors with integrated magnetic concentrator (IMC) has increased [7]. Figure 3.5 shows the way in which these Hall sensors operate. A single-axis IMC-Hall sensor consists of a Hall element and an electronic circuit that has a thin structured ferromagnetic layer on the surface. A magnetic field $\vec{H}$ is parallel to a chip surface is rotated locally to a vertical direction under the edges of the IMC close to the gap. It can now be measured by the Hall element. The IMS also plays the role of a passive amplifier.

The sensitivity, which can be achieved with the IMC-Hall sensors, is a hundred times higher than that of convenient Hall sensors. For example the sensitivity of chip 1SA-1V developed by *SENTRON* AG (Switzerland) is about 300 V/T. The bandwidth is 0-100 kHz.

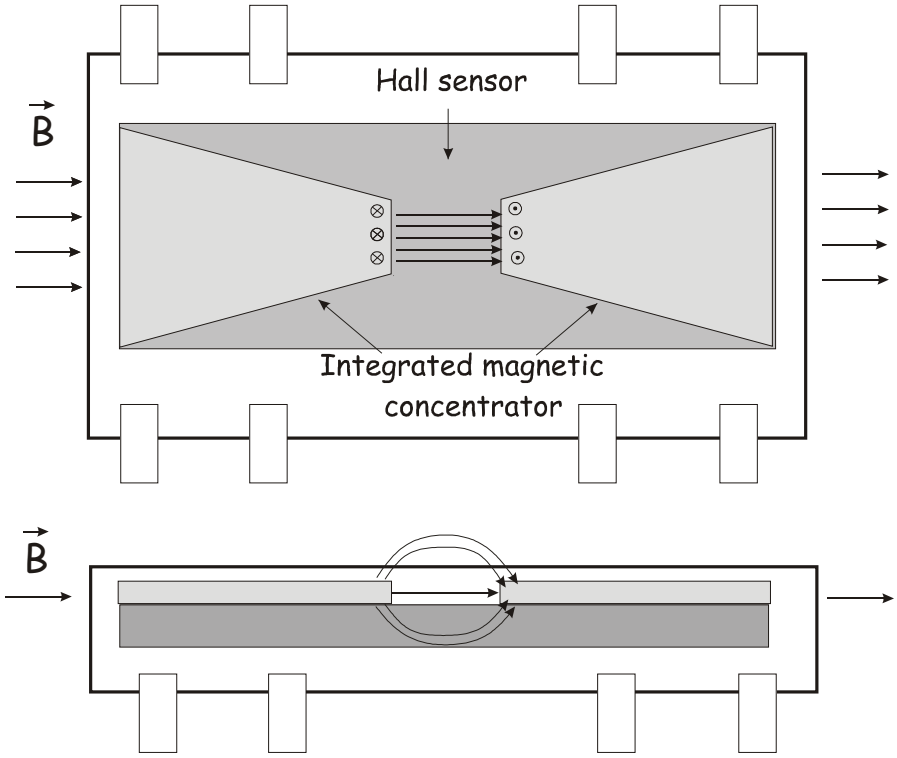

Fig. 3.5. The principle scheme of IMC-Hall chip.

3.2.2. The AMR sensor.

The magnetoresistive effect is the change of the resistivity of a material due to a magnetic field. Thompson discovered it in 1856. Later, with the improvement of the technology of thin ferromagnetic films, the anisotropic magnetoresesestive effect was observed. The resistivity of the thin ferromagnetic strip, for example the Permalloy, depends on the angle between its magnetization and the electrical current flow. The maximum change of the resistivity in the presence of a magnetic field is about 2-3%.

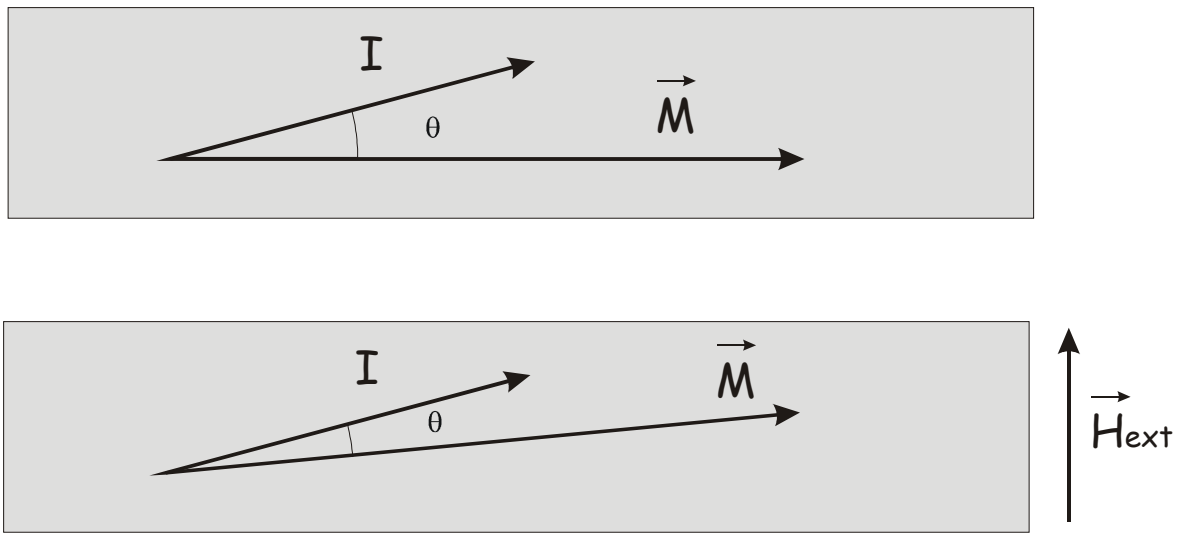

Fig. 3.6. The Permalloy strip has a magnetization vector $\vec{M}$. The applied magnetic field changes the orientation of magnetization vector $\vec{M}$. The resistance of the film changes as a function of the angle between the vector $\vec{M}$ and a current flowing through it.

As shown in Figure 3.6, the magnetization vector $\vec{M}$ has been set parallel to the length of the strip (during manufacturing) and the current flow has the angle θ to the length of the strip. An external magnetic field causes the magnetization vector to rotate and change the angle θ. This will cause the resistance value to vary. The dependence of the resistance can be described by the empirical formula (3.4) [8].

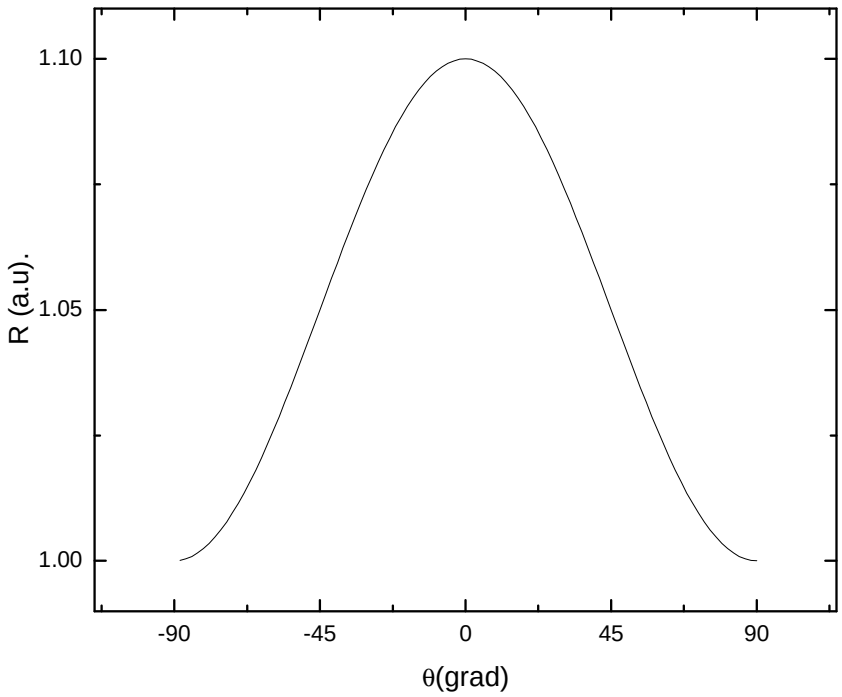

Fig. 3.7. This curve shows how the resistance of the Permalloy film changes with the angle θ between the direction of the current and the direction of the magnetization.

$$R(\theta) = R_0 + \Delta R \cdot \cos^2(\theta), \qquad (3.4)$$

where R_0 is the resistance perpendicular to the magnetization, and ΔR is the maximum change of resistance due to the magnetic field. Figure 3.7 shows the dependence of the resistance on the angle θ.

One can see from formula (3.4) and Figure 3.7 that the dependence of the resistance is strongly non-linear, but there is a linear region at about the 45º angle. To achieve this linear region it is necessary to shift the whole curve to 45º grad. The method used to cause the current to flow at a 45º angle to the long axis of the strip in the film is called the barber pole biasing. It is accomplished through a layout technique that places low-resistance shorting bars across the film's width at a 45º angle. The current, preferring to take the shortest path between two shorting bars, thus flows from one bar to the next. Once the shorting bars have been placed at a 45º angle, the direction of the current can be held at a 45º angle to the length of the strip.

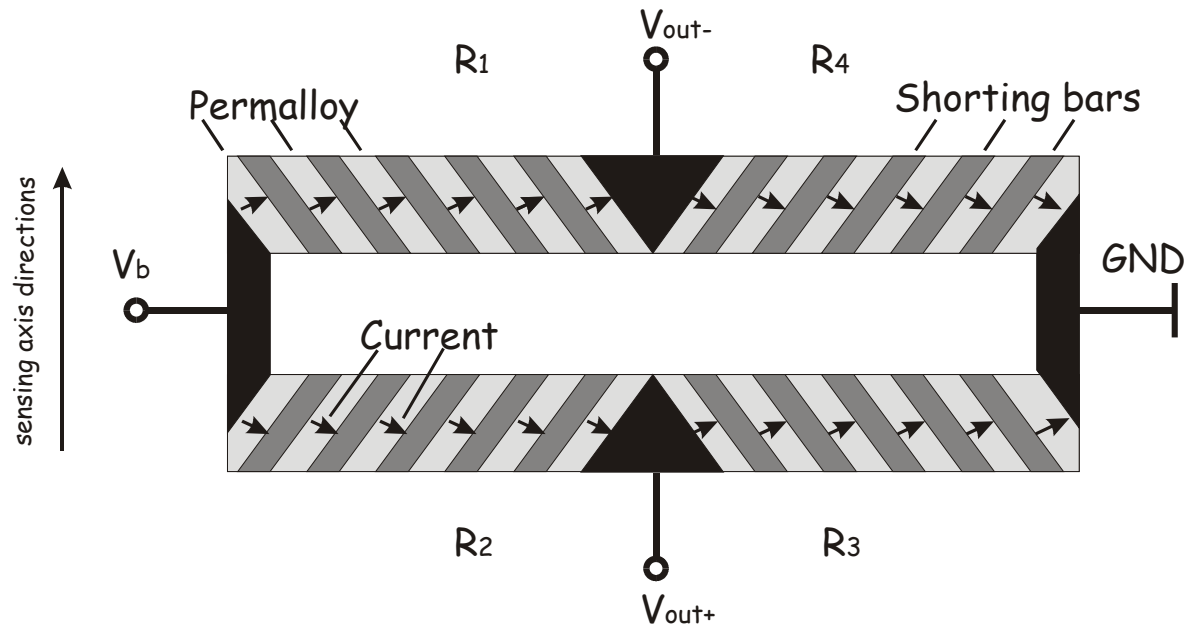

Fig. 3.8. The structure of the single axis AMR sensor. The four Permalloy strips in a Wheatstone bridge are connected. V_b is the bridge operating voltage. The voltage difference between V_{out-} and V_{out+} is proportional to the applied magnetic field.

Commonly four Permalloy strip resistors are deposited on the silicon base in a Wheatstone bridge and are connected. Figure 3.8 shows the structure of the single axis AMR sensor. The barber pole structure of the resistors included in a bridge is made in such a way that an external magnetic field causes an increase of resistance in the right bridge arm (resistors R_4, R_3), and a decrease of resistance in the left arm (resistors R_1, R_2) of the bridge. Thus, the output voltage of the bridge is proportional to the applied magnetic field.

The bridge sensitivity S, is expressed in mV/V/T, where the middle term V is a bridge operating voltage. For example, the sensitivity of the AMR sensor HMC1001 that is manufactured by Honeywell [9] is 40 V/V/T. It gives the sensitivity 400 V/T of the sensor for a bridge operational voltage equal to 10 V. The AMR sensor HMC1001 has a bandwidth of 0-5 MHz.

The AMR sensors have several advantages, like high sensitivity and a wide bandwidth, but they have also several disadvantages. For instance, since the magnetic field is more than 1mT, when it is applied along the length of the strip, it could upset, or flip, the magnetization of the Permalloy strip, thus changing the sensor characteristics. If the magnetizagion of the Permalloy strip

is upset, a strong magnetic field must be applied momentarily in order to restore, or set the sensor characteristics. There are specially integrated coils in the device, which set or reset the magnitization of the sensor.

There is also a problem with the AMR bridge offset due to the resistors' mismatch during the manufacturing process. This offset can be trimmed to zero by adding the shunt resistor across one arm of the bridge to force both outputs to the same voltage. This must be done in a zero magnetic field environment, usually in a zero gauss chamber. The AMR sensors manufactured by Honeywell have one interesting options. Due to the manufacturing of the sensor the OFFSET strap is made. With the help of this strap any ambient magnetic field can be cancelled by driving a defined current through the OFFSET strap. This technique can be used, for example, for eliminating the remanence magnetic field of the magnetic yoke in the magnetic flux concentrator. The more detailed information about the features of the Honeywell AMR sensors can be found in application notes [9].

3.2.3. The GMR Sensor.

Recent developments in thin-film magnetic technology have resulted in films exhibiting a large change in resistance with a change in the magnetic field. This phenomenon is known as the giant magnetoresistance (GMR) to distinguish it from conventional anisotropic magnetoresistance (AMR). Whereas AMR resistors exhibit a change of resistance of less than 3 %, various GMR materials achieve a 10 to 20 % change in resistance. GMR films have two or more magnetic layers separated by a non-magnetic layer. Due to spin-dependent scattering of the conduction electrons, the resistance is maximum when the magnetic moments of the layers are antiparallel and minimum when they are parallel [10].

Several companies currently manufacture the commercially available GMR sensors. For example the material used in GMR sensors manufactured by NVE corporation is called an unpinned sandwich. Unpinned sandwich GMR materials consist of two soft magnetic layers separated by a layer of a non-

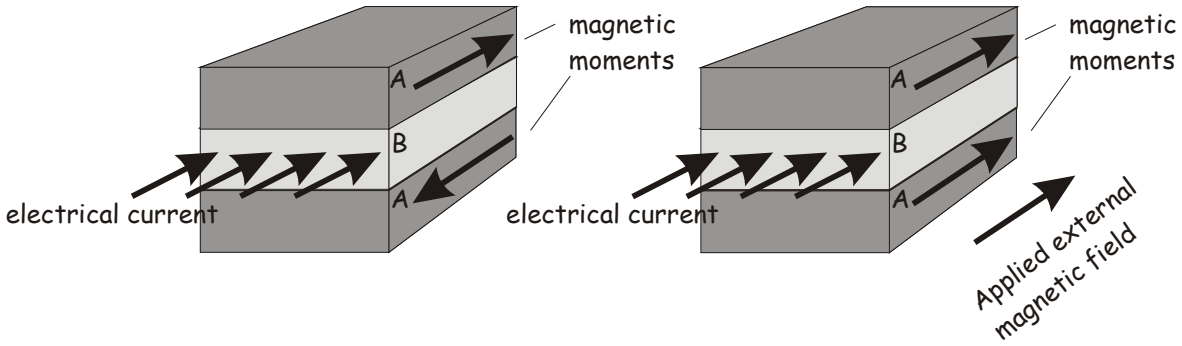

Fig. 3.9. Unpinned sandwich. The dark grey layers *A* are the ferromagnetic material. The light grey layer B is the current-carried, non-magnetic, highly conductive material.

magnetic conductor such as copper. With magnetic layers of 4 to 6 nm (40 to 60 Å) thickness separated by a conductor layer typically 3 to 5 nm thick there is a relatively little magnetic coupling between the layers. Figure 3.9 illustrates the structure of the GMR film.

The magnetic field caused by an electrical current in a layer of a non-magnetic conductor flowing along the strip is sufficient to rotate the magnetic layers into antiparallel or high resistance alignment. An external magnetic field applied along the length of the strip is sufficient to overcome the magnetic field from the current, as well as overcoming any magnetic exchange interaction between the layers, and is able to rotate the magnetic moments of both layers parallel to the external field thereby reducing the resistance of the film. Both a positive and a negative external field parallel to the strip will produce the same change in resistance.

Thin-film GMR materials deposited on silicon substrates can be fabricated to form Wheatstone bridges. A sensitive bridge is fabricated from four photolithographically patterned GMR resistors, two of which are active elements. Figure 3.10 shows small magnetic shields of permalloy, plated over two of the four equal resistors in a Wheatstone bridge. The Permalloy shield protects these resistors from a measured magnetic field and allows them to act as reference resistors. Since the resistors are fabricated from the same material, they have the same temperature coefficient as the active resistors. The two

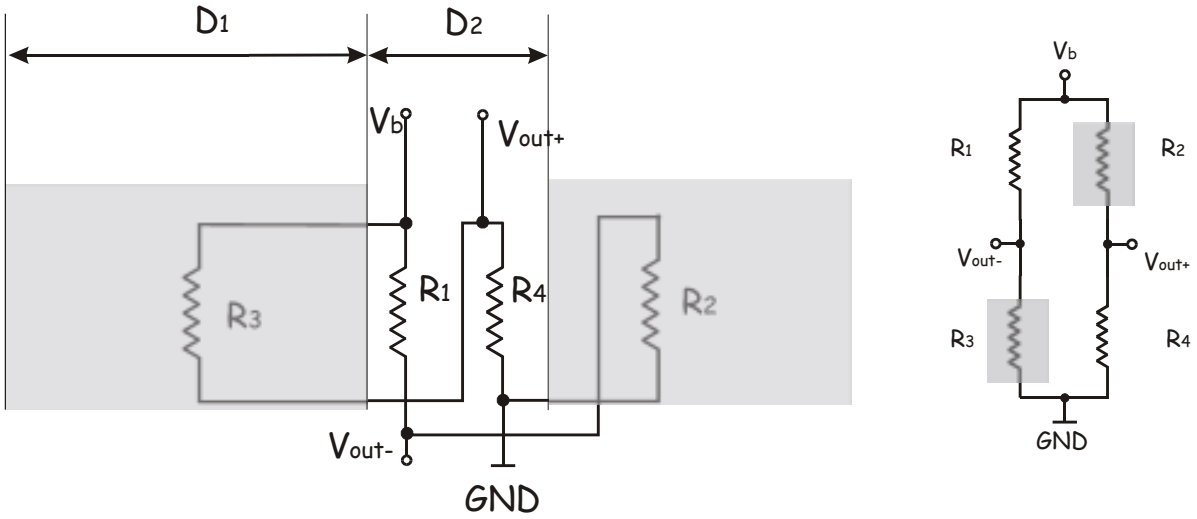

Fig. 3.10. The scheme of a GMR sensor. The transparent grey squares are the Permalloy shieldings of the reference resistors and act as the flux concentrator.

remaining GMR resistors are both exposed to the external magnetic field. Additionally, the Permalloy structures that are plated onto the substrate can act as flux concentrators to increase the sensitivity of the bridge. The active resistors are placed in the gap between the two flux concentrators. These resistors experience a magnetic field that is larger than the applied magnetic field by, approximately, the ratio of the gap between the flux concentrators, D1, and the length of one of the flux concentrators, D2.

The commercially available GMR sensors manufactured by NME have a typical sensitivity of about 40 V/V/T, and a bandwidth of 0-1 MHz.

3.2.4. The comparison of the magnetic field sensors.

The table bellow shows the typical characteristics of the four different kinds of magnetic field sensors.

Characteristics	Unit	AMR	GMR	IMC-Hall	Hall
Sensitivity	V/T	400	400	300	1
Field Range	mT	-0.6 / +0.6	-3.5 / +3.5	-10 / +10	-1000 / +1000
Disturbing Field	mT	2	100	-	-
Bandwidth	MHz	0-5	0-1	0-0.1	0 - 0.1
Linearity Error	%FS	0.4	2	0.5	-
Hysteresis Error	%FS	0.08	2	0.005	-
Offset	mV	5	20	0.01	-

The AMR kind of magnetic field sensor is more suitable for the purpose of the magnetic flux concentrator because of its sensitivity and its bandwidth. The Hall sensor is not suitable because of its small bandwidth and its lower sensitivity. The IMC-Hall sensors are not suitable because of their small bandwidth. AMR and GMR sensors have one important parameter– disturbing field value. The magnetic field of this value applied to the sensor will damage a sensor. The AMR sensors have integrated set/reset coils which can restore the characteristics of the sensor after the distortion caused by a high magnetic field. However, the GMR sensors will be irreversible damaged by a high magnetic field. The GMR sensors also have a much bigger hysteresis error in comparison wit the AMR sensors. The integrated Honeywell sensor's OFFSET corrections can help to eliminate the influences of the external magnetic field and the remanence magnetic field of the magnetic flux concentrator yoke.

4. MAFIA calculations.

The main part of the magnetic flux concentrator is a magnetic yoke in form of a torus with a rectangular cross section and a small air gap for a magnetic field sensor. The magnetic flux is mainly concentrated in the material of the yoke with high permeability. The three-dimensional magnetic flux distribution one can find by solving the Poisson equation for the vectorial potential. There are good developed methods for the solution of magneto-static problem with axially symmetrical magnetic material distribution in terms of a convergent power series, but the presence of the air gap destroys the axial symmetry and makes an analytical solution of the problem almost not possible. Therefore it is necessary to perform a numerical simulation.

For the simulation of the magnetic flux distribution in the magnetic flux concentrator yoke the program package MAFIA of the German software company “CST” was chosen. Since the first realisation of this program package in 1983, MAFIA is in use in different laboratories and institutions for solving of various electromagnetic problems.

4.1. About MAFIA.

MAFIA (**MA**xwell's equations by the **F**inite **I**ntegration **A**lgorithm) is an interactive program package for the computation of electromagnetic fields. It is based directly on the fundamental equations of electromagnetic fields, Maxwell´s equations [11]. The basis of all computations is the theory of the discrete Maxwell-grid-equations, the so-called Finite Integration Technique, which has been developed during the last twenty years. This theory formulates Maxwell´s Equations in form of algebraic matrix equations. The matrices fulfil the same formal relations as the differential operators in the basic field equations. The vector solutions on the grid possess the same physical properties as the electromagnetic fields.

MAFIA 4.112 is a modular program package. It is divided in pre-processor, postprocessor and solvers for different special cases of Maxwell´s equations. The program package consists of the following modules:

- M: Pre-processor includes solid modeller, CAD import, and 3D graphics.
- P: Postprocessor includes 3D graphics and calculations of deduced quantities like path integral or impedance
- S: Static field module, solves electrostatics, magnetostatics, heat flow problems, stationary current flow problems, and electro-quasistatic problems
- T3: Time domain module, simulates time dependent wave propagation, most general and versatile in application. Uses Cartesian coordinates.
- TS3: Time domain module, simulates charged particle movement in time dependent fields including the interaction of the particles and the fields. Uses Cartesian coordinates only.

- TS2: Time domain module, simulates charged particle movement in time dependent fields including the interaction of the particles and the fields in cylinder symmetrical structures.
- E: Frequency domain eigenmode module, finds modes in resonators and wave-guides.
- W3: Frequency domain module covers the whole frequency range.
- H3: Thermodynamic module, solving thermodynamic problems in time domain in either Cartesian or polar coordinate system.
- T2: Time domain module, simulates time dependent wave propagation within cylinder symmetrical structures.
- A3: Time domain acoustic solver.
- OO: The optimisation driver is composed of actually all MAFIA's modules. It provides the effective communication between the above mentioned eleven modules within the MAFIA project.

There are two modes of MAFIA operation, a GUI (Graphical User Interface) and a command line mode. The command line mode is realized within the OO optimisation driver. The optimisation driver provides access to all MAFIA modules. The GUI is a relative new part and not yet supports all features. Originally the program package MAFIA exists only for big computer workstations, but with the growth of the PC's performance and the popularity of MS Windows the company CST issued a version of MAFIA for MS Windows.

4.2. The model.

The following parameters for the dimensions of the toroidal yoke where defined: the inner radius is 100 mm, because the device must fit around the beam pipe, the outer radius is 125 mm, the height is 30mm, and the air gap is 5mm. The beam current is modelled as straight line current with a length much bigger as the height of the torus. The first task before calculating a magnetic field distribution, the same as for any electromagnetic problem solving with MAFIA, is the modelling of the material distribution within a computation volume. Afterwards for the application the of finite integration algorithm, it is necessary to divide a computation volume into small cells, the so-called mesh. This discretization, roughly speaking allows to reduce the problem of solving the partial differential equations to solving of a big system of linear algebraic equations. After the mesh creation one can use the appropriate solver for a given physical problem.

For the present calculation the command line mode of MAFIA is chosen. The command line mode means you need to “say” MAFIA what you want to do by typing certain MAFIA commands. To get this operation mode it is necessary to start the MAFIA module OO-the optimization driver. To avoid unnecessary typing of repeating commands one can type the whole necessary sequence of commands for modelling a material distribution and calculation in a text editor and than copy this script to the command line via clipboard.

First of all it is necessary to define the computation volume that will contain the model of yoke and current. This volume must be bigger than the model of the yoke to avoid side effects in the computations. It spreads from -200 mm up 200 mm in X direction, from -200 mm up 200 mm in Y direction and from -100 mm up 100 mm in Z direction. The material distribution is centred in the origin of the coordinate system. The MAFIA provides standard for any CAD program mechanism of a new shape creation. With the help of the binary operations as union or intersection one can combine a simple geometrical forms

like the cylinders, the spheres, the cones, the torus, the washers and the rectangular bricks. One can invert the shape, than the inverted shape consists of the whole computation volume except the volume of the original shape. The model of the yoke is intersection of the washer, and the inverted brick. The axis

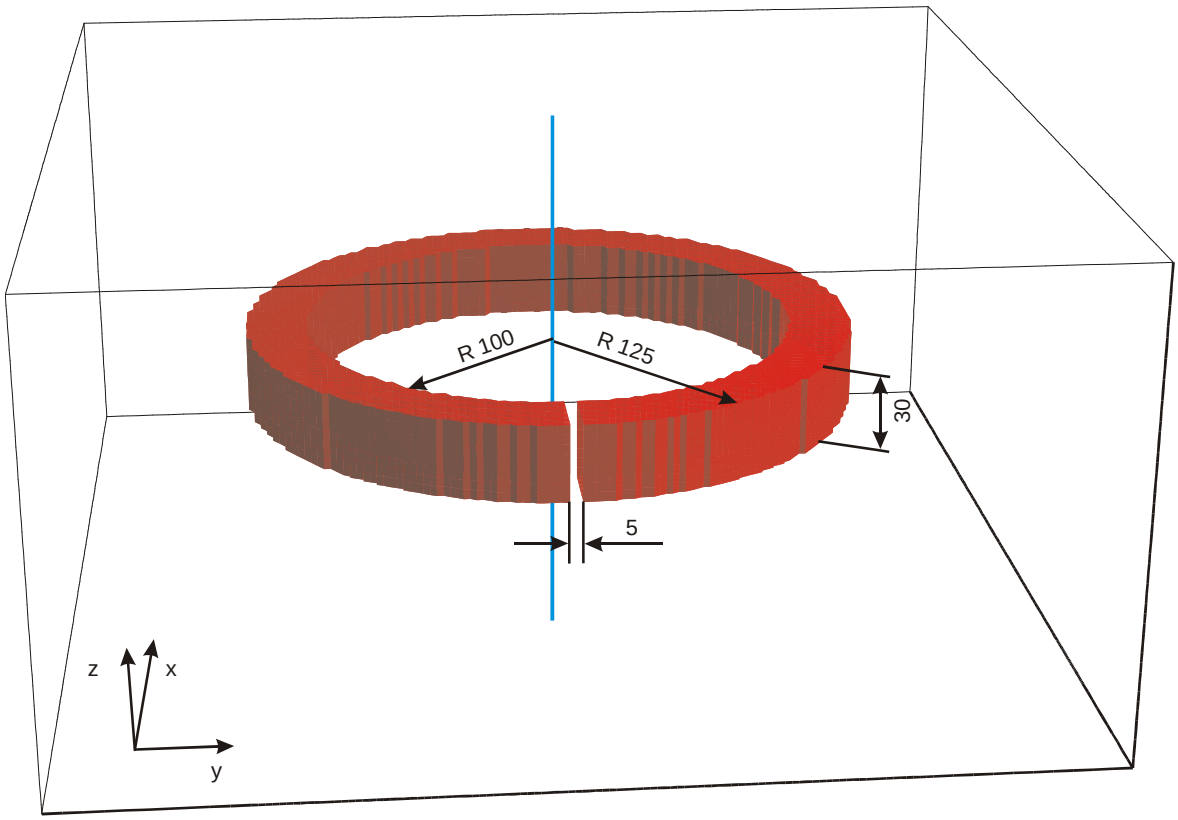

Fig. 4. 1. A view of the calculation volume. The black wire box is the boundary of the computation volume, the red washer with the gap is the yoke from magnetic material, and the blue line represents a current.

of the washer along the Z axis of coordinate system is oriented. Also an important part of the model creation is the definition of the excitation current. In MAFIA terms a current calls a filament. This procedure has one trick. The current ends must exceed the computation volume. Figure 4. 1 shows the computation volume, the model of yoke and excitation current.

An important part of the model creation is meshing the computation volume into small cells. Figure 4.2 shows the mesh cells in plane $Z = 0$. MAFIA provides a wide range of meshing procedures. One can create the mesh automatically, and then it produces a homogeneous mesh, or one can specify

variable densities for automatically created meshes and one can create the mesh "manually" by defining the coordinates range and number of mesh lines in this

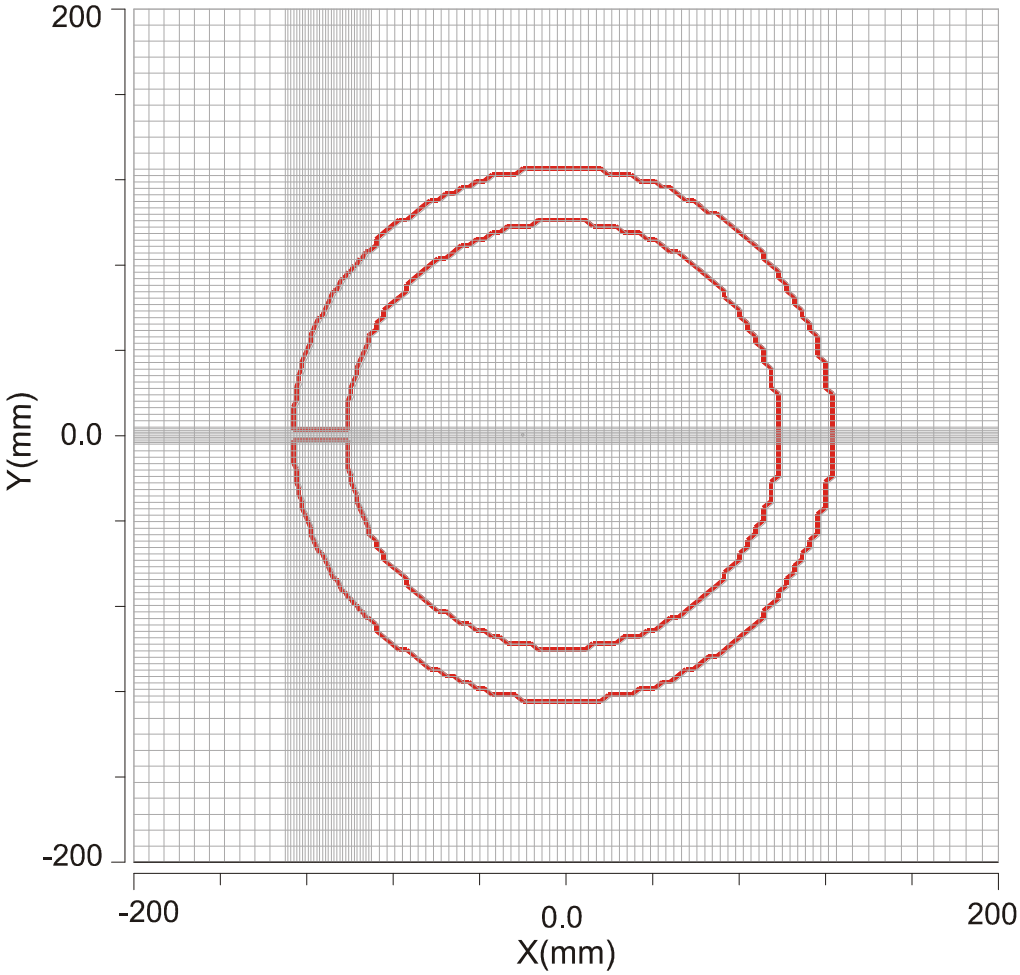

Fig. 4.2. The 2D view of the yoke model and mesh cells in XY plane.

range. For the present model the mesh is created "manually". The mesh density is not a constant within the computation volume. One can distinguish three different mesh densities. The mesh is denser in the yoke material than in the empty space, and the densest mesh is near placed the air gap. The whole mesh has about 10^6 cells. Now the creation of the model is finished and the model is prepared for calculation.

4.3. The calculations.

Now it is necessary to define the properties of the material and the boundary conditions. Depending on a physical problem one may define a dielectric permittivity or a magnetic permeability for the static problem solver, or the high frequency dielectric permittivity for the eigenmode solver or the transient solver. Thus in the static solver module the magnetic properties of a material, the magnitude of the electrical current and the boundary conditions will be defined. The term “boundary conditions” for numerical calculations has another meaning than for an analytical calculation. In an analytical calculation it is necessary to define the conditions for the fields on the interface between two different mediums, whereas for numeric simulations it is necessary to define conditions at the boundary of the computation volume, i.e. how the solution should behave at the boundary of the computation volume. MAFIA provides the following types of boundary conditions:

- Normal: Set the potential of the boundary of the computation volume to a fixed value.
- Tangential: Set the normal derivative of the potential to zero at the boundary of the computation volume.
- Open: Causes the program to approximate an open boundary of the computation volume to a free space.

The future device will operate within a magnetic shielding. This means that in the space within the magnetic shielding there are no external magnetic fields. Therefore the last boundary conditions are chosen for the simulation of the magnetic flux concentrator.

MAFIA can operate with both a linear magnetic medium and with a none-linear, but cannot take into account a hysteresis effect such a remanence. For the purpose of creating a magnetic flux concentrator the extreme high permeable ferromagnetic medium VITROVAC 6025F as yoke material is chosen. In order to calculate the response function of the device on the excitation current it is

necessary to take into account the non-linear field-flux dependence. The relative magnetic permeability of the computation volume is set equal to 1. To define the

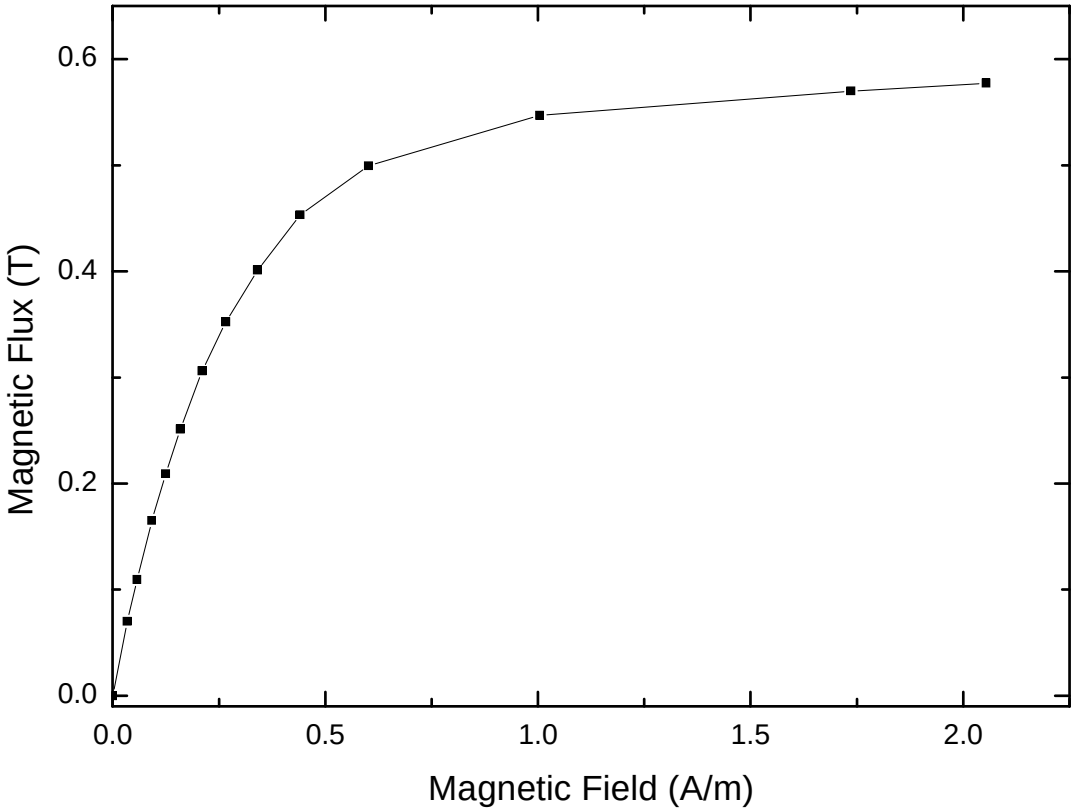

Fig. 4. 3. The non-linear dependence of the magnetic flux in dependence of the magnetic field for VITROVAC 6025F. Black squares are experimentally measured values.

magnetic properties of the yoke the non-linear field-flux dependence of material is specified in table form. Figure 4.3 shows this dependence for VITROVAC 6025F. This curve was measured in order to design another devices such as ac- and dc-transformer at GSI. From this data MAFIA calculates the relative permeability of the material.

4.4. Results.

The calculation of the magnetic field was made using a personal computer with an AMD 1600XP processor and a RAM of 256MB. The calculation time for non-linear problems depend on the strength of the magnetic field and thus from the excitation current. For small currents, which caused a magnetic flux that is far away from saturation, the calculation takes about 5 minutes of CPU time. For a bigger current, which causes a magnetic filed flux near a saturation the calculation takes about 10 minutes of CPU time. The MAFIA post processor

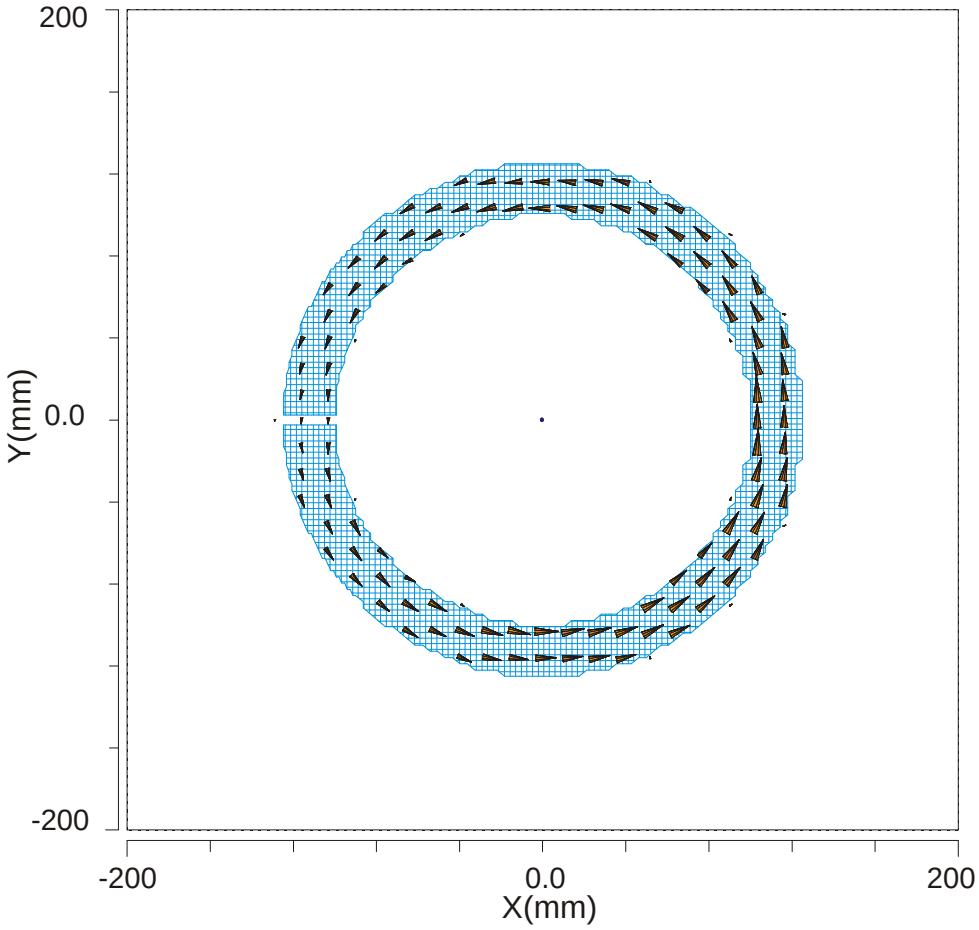

Fig. 4.4. The 2D arrow plot of the magnetic flux for an excitation current of 10A, the small blue spot is the current placed in the origin of the coordinate system. The arrow size defines the magnetic flux strength; the arrow direction corresponds to magnetic flux direction.

module provides a wide range of graph types, 2D arrow plots, 3D arrow plots for vector fields, as well as hill plots and contour plots for scalar fields. Figure

4.4 shows a 2D arrow plot of the magnetic flux for an excitation current of 10 A. One can see that the magnetic flux in the magnetic yoke only is concentrated. The field has only the tangential to the yoke boundary component.

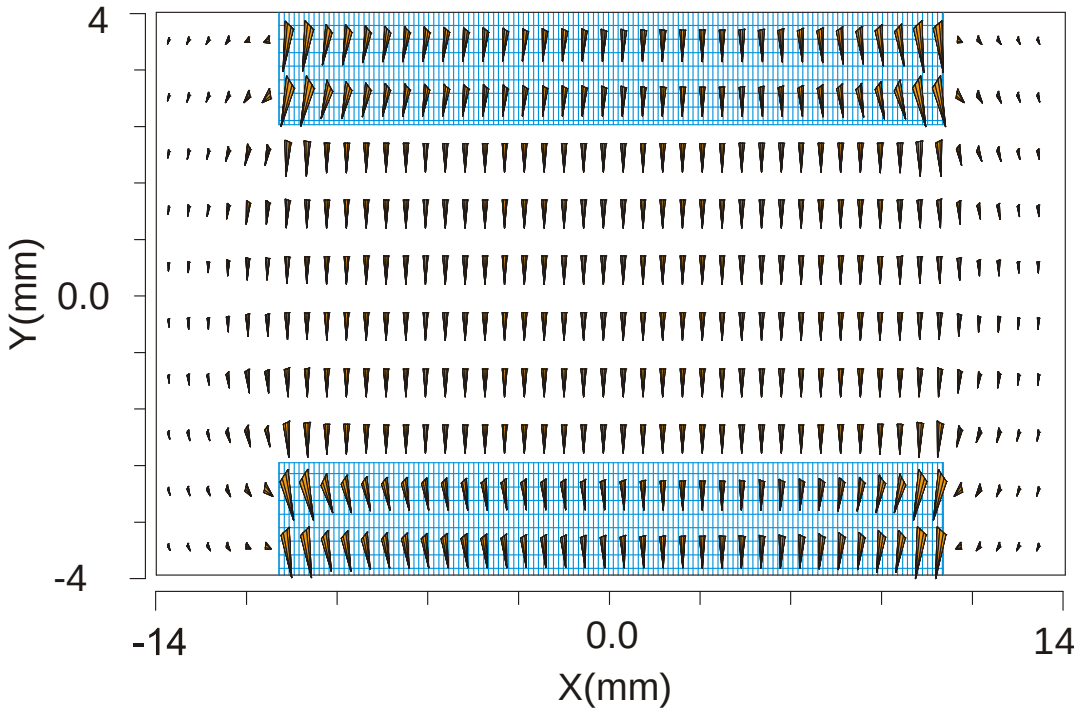

Fig. 4.5. The arrow plot of the magnetic flux field in the air gap area, the origin of the coordinate system corresponds to the air gap centre. The arrow size defines the magnetic flux strength; the arrows direction corresponds to the magnetic flux.

Because all magnetic sensors are only able to measure one component of the magnetic flux, the homogeneity of the magnetic flux within the air gap is important. Figure 4.5 shows the magnetic flux vectors within the air gap, the field is mostly the perpendicular to the gap poles and it slightly disturbed in the closeness of the poles corners. Thus the field within the air gap can be easily measured with any type of magnetic flux sensors.

The arrow type plot is good for qualitative analysis, but to use such a graph for the extraction of quantitative information is not adequate. The absolute value of the magnetic flux is more suitable for quantitative analyse. Figure 4.6 shows the contour plot of the magnetic flux absolute values. With the help of the attached colour scale one can encode the absolute value of the magnetic flux.

One can see from Figure 4.6 that the maximum value of magnetic flux in the yoke material is about 10^{-2} T, that is far away from the saturation value equal to

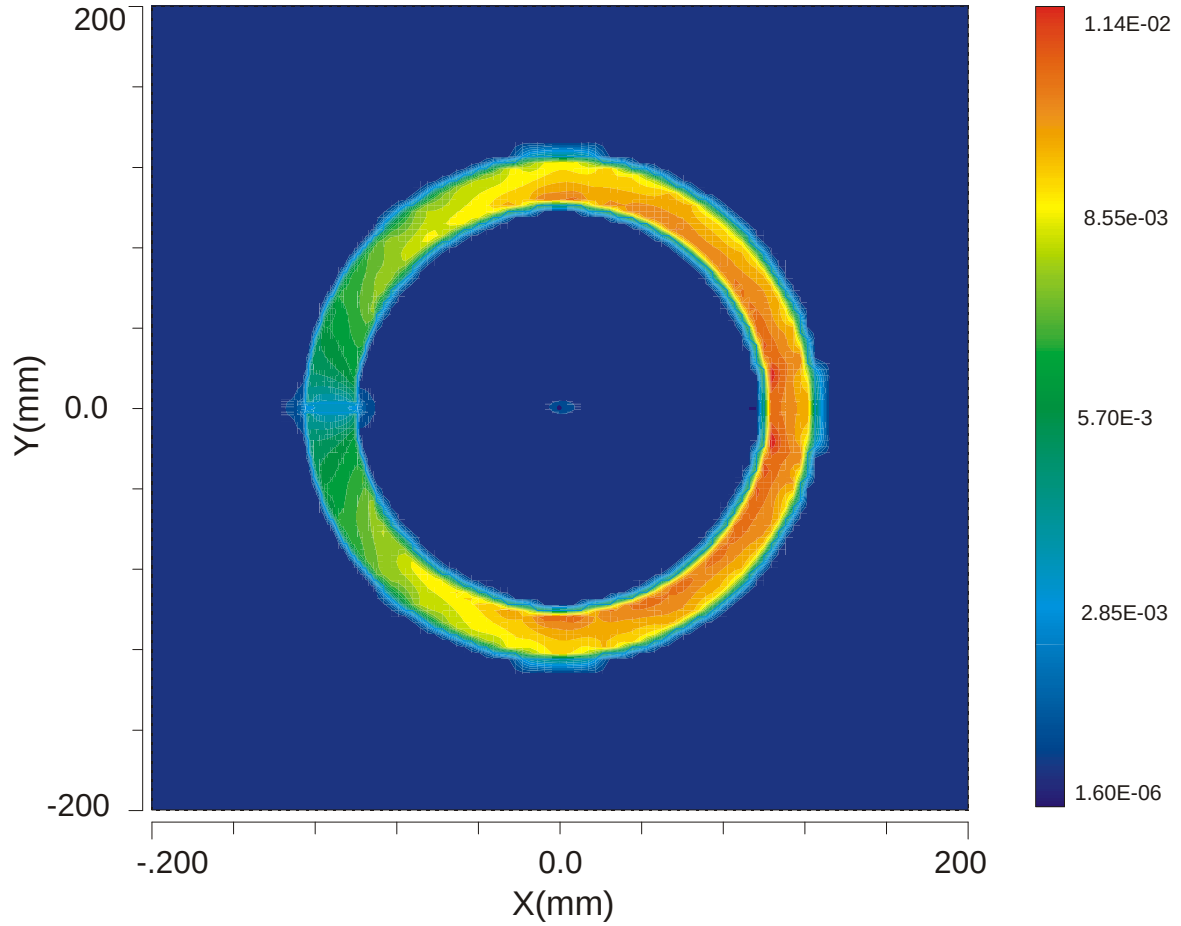

Fig. 4.6. The contour plot of the magnetic flux absolute values an for excitation current of 10 A. The aligned colour scale is in T. The hot colours correspond to high absolute values of the magnetic flux; the cold colours correspond to small absolute values of the magnetic flux.

0.5 T. For comparison Figure 4.7 presents the magnetic flux absolute values for a yoke without air gap with the same value of the excitation current. One can see that the same excitation current caused a saturation of the magnetic yoke. This fact can be easily understand with the help of Ampère's law (4.1)

$$\oint_L \vec{H} \cdot d\vec{l} = I\,, \qquad (4.1)$$

where $\vec{H}$ is the magnetic field, L any closed contour passing the air gap and lying within the torus, I is a current passed through the contour L. Firstly consider the case of a yoke without an air gap. For simplicity the contour L as

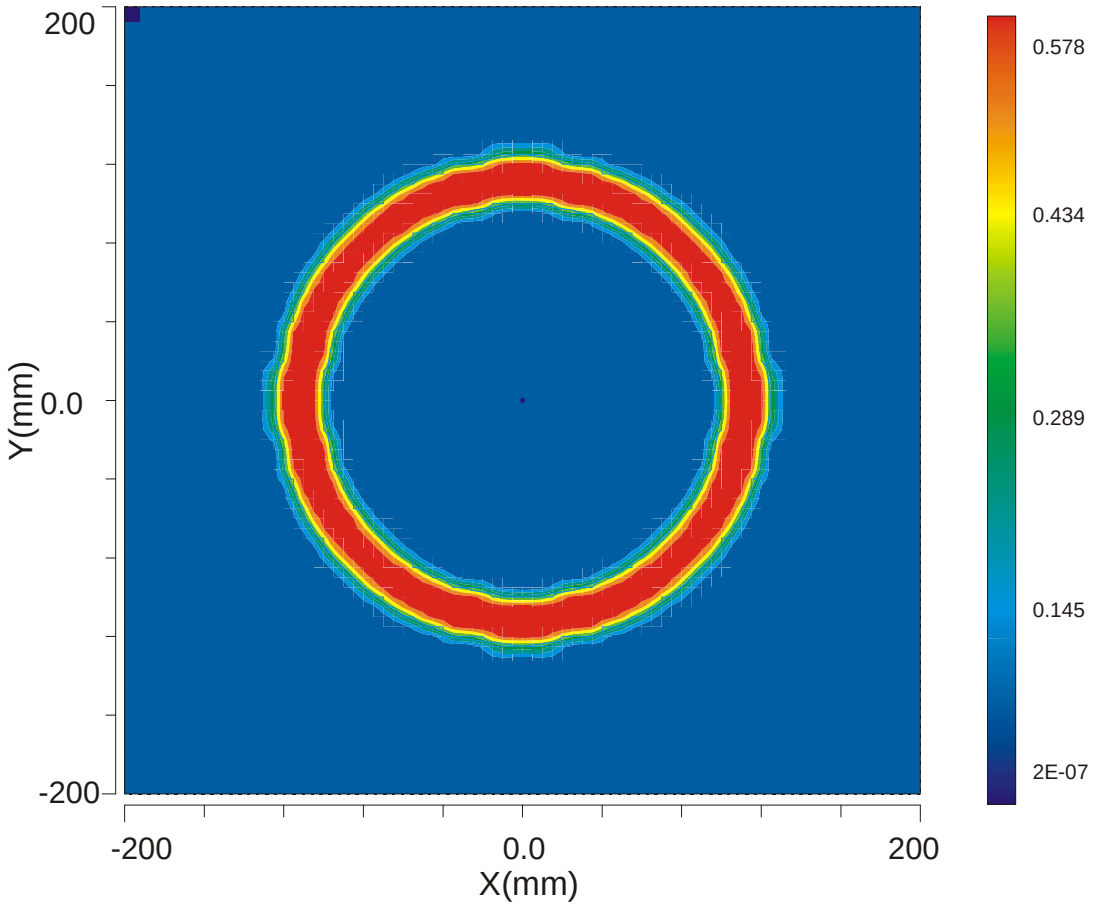

Fig. 4.7. The contour plot of magnetic flux absolute value for excitation current 10 A. The aligned colour scale is in T. The hot colours correspond to high absolute value of magnetic flux, the cold colours correspond to small absolute value of magnetic flux.

the circle lying within the yoke is chosen. In suggestion that $\vec{H}$ is constant along the contour L one can obtain from Ampère's law 4.1 as the next expressions for the absolute value of the magnetic field.

$$H = \frac{I}{2\pi R} \tag{4.2}$$

For a circle of a radius of 0.11 m and a current of 10 A Formula 4.2 gives us a value of the magnetic field of 14.46 A/m. From the field-flux curve presented in Figure 4.3 one can see that this value causes saturation of the magnetic material. This fact is in agreement with results of numerical simulations presented in Figure 4.6. For the case of the yoke with the air gap the contour L consists of straight line within the air gap and a part of a circle within the yoke. Despite the fact that the magnetic field is no more constant along the curve within the yoke one can make the estimation in the same way as for the previous case. Let the

magnetic field $\vec{H}_1$ be constant in the yoke. Let the magnetic field $\vec{H}_2$ be constant in the air gap, L_1 and L_2 are curve and linear part of the whole contour L. Applying of Ampère's law to this case lead to the formula 4.3

$$H_1 \cdot L_1 + H_2 \cdot L_2 = I\,. \tag{4.3}$$

The fields $\vec{H}_1$ and $\vec{H}_2$ are connected via the boundary condition

$$H_{1n} = \frac{\mu_2}{\mu_1} H_{2n}, \tag{4.4}$$

where μ_1 and μ_2 are the permeabilities of air and the yoke material respectively. Thus from formulas 4.3 and 4.4 the magnetic field in the yoke material H_2 is equal to:

$$H_2 = \frac{I}{\frac{\mu_2}{\mu_1} L_1 + 2\pi R}, \tag{4.5}$$

where L_1 is the length of the air gap and R is the radius of the circle. The formula 4.5 shows that the value of the magnetic field in the yoke material can be controlled by the $\frac{\mu_2}{\mu_1}$ ratio, which is for the present case the relative permeability of the yoke material or by the length of air the gap L_1. For R equal to 0.11 m, current I equal to 10 A and with the $\frac{\mu_2}{\mu_1} = 10^6$ formula 4.5 give the value of the magnetic field within the yoke of about 10^{-3} A/m. This value of the magnetic field according to the flux-field data from Figure 4.3 corresponds to the magnetic flux value of about 10^{-3} T. It is also in agreement with simulations that show the same order of magnitude of the magnetic flux within the yoke.

In order to ascertain the dependence of the magnetic field within the air gap on the current position two series of simulations are performed. In the first series the current position varies in both negative and positive X directions and

the. Y coordinate stays equal to zero. In the second series the current position varies in both negative and positive Y directions and the X coordinate stays equal to zero. Such series of simulations for value of excitation current equal to 10 A is made. The results are presented in Figures 4.8 and 4.9.

One can see from the Figures 4.8 and 4.9 that a relative inaccuracy of the

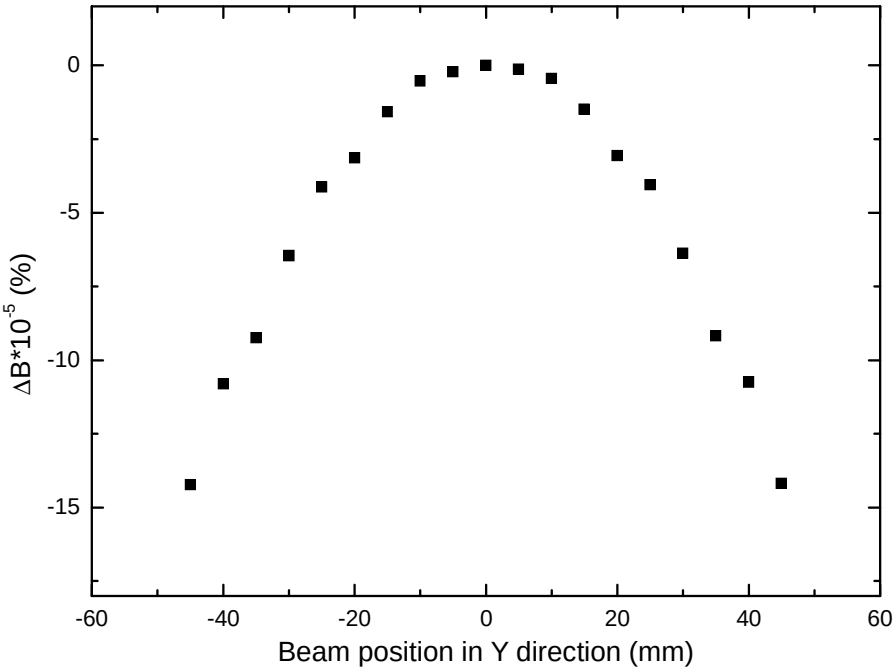

Fig. 4.8. The relative change of the absolute magnetic flux value in the centre of the air gap in percent as a function the beam position variation in Y direction for a beam current of 10 A.

current measurement by the magnetic flux concentrator due to the variation of the beam position is about some 10^{-5} percent. This result is valid not only for a beam current equal to 10 A, but also for current from 1 mA up to 100 A. This fact follows from the linearity of the response function presented in Figure 4.10.

Because the sensitive area of the magnetic field sensor is small the homogeneity of the magnetic flux distribution is important. Figures 4.11 and 4.12 show the relative changes of the absolute magnetic flux values in two perpendicular planes.

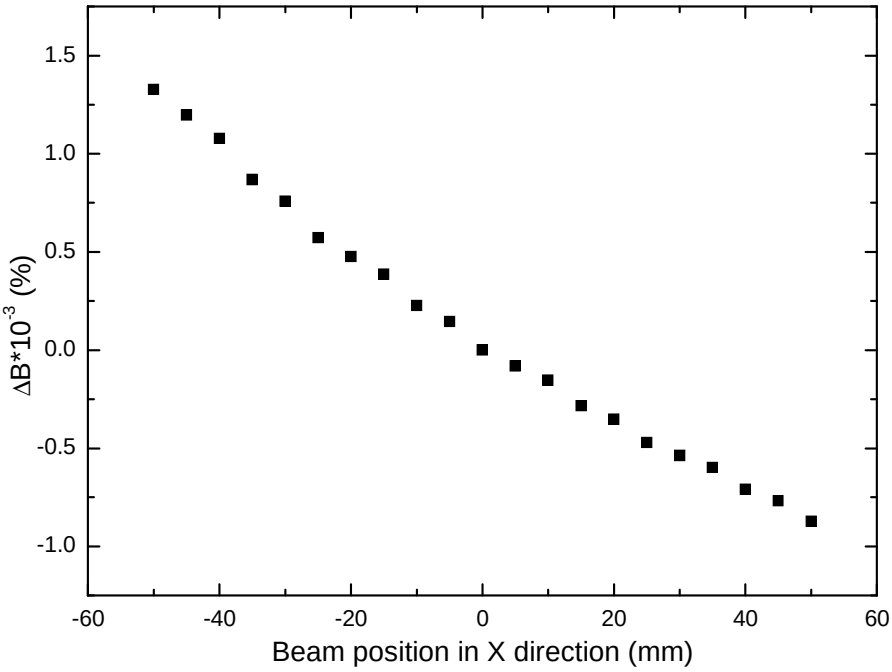

Fig. 4.9. The relative change of the absolute magnetic flux value in the centre of the air gap in percent as a function of the beam position variation in X direction for a beam current of 10 A.

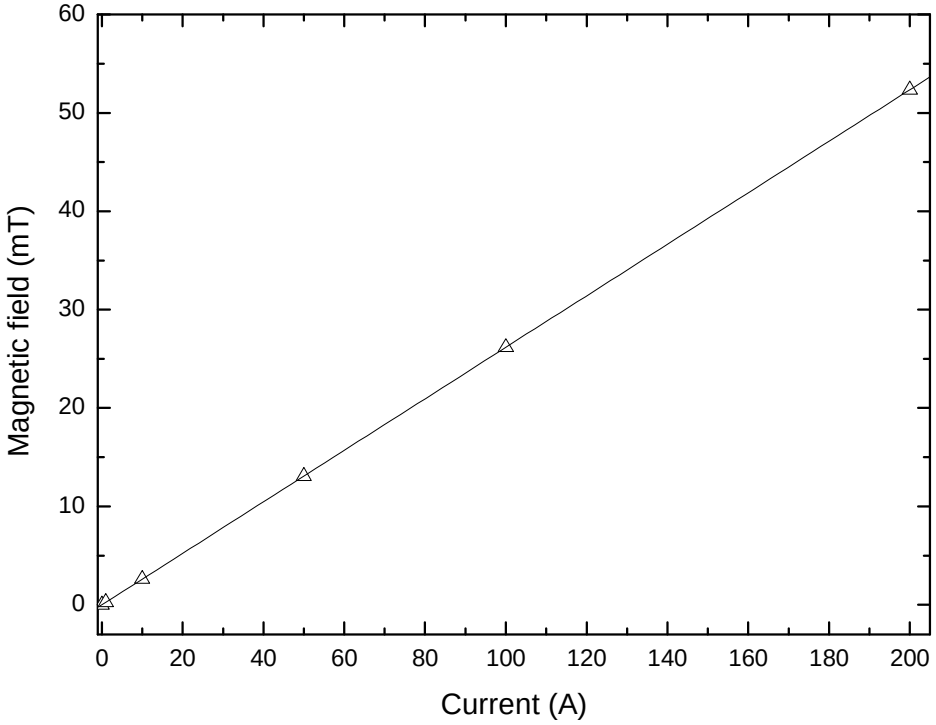

Fig. 4.10. The dependence of the absolute magnetic flux value in the air gap on the excitation current. The straight line is a linear fit of the data obtained in the simulations.

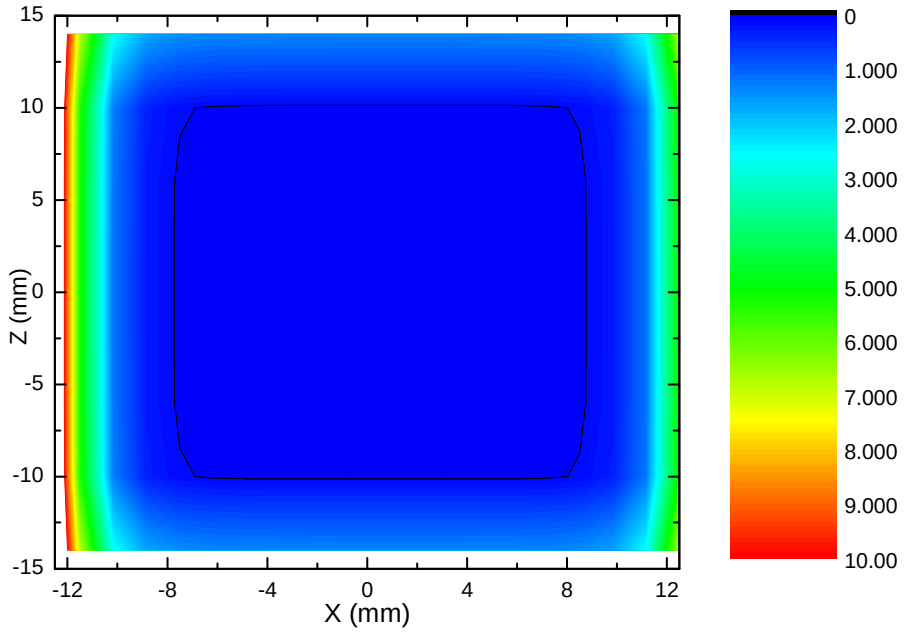

Fig. 4.11. The distribution of the relative changes of the absolute magnetic flux value. The origin of the coordinate system corresponds to the air gap centre. The hot colours correspond to big relative changes; the cold colours correspond to small relative changes. The whole colour scale corresponds to relative changes about 10 percent. The area surrounded by the black line has relative changes of the flux within less than 0.1%.

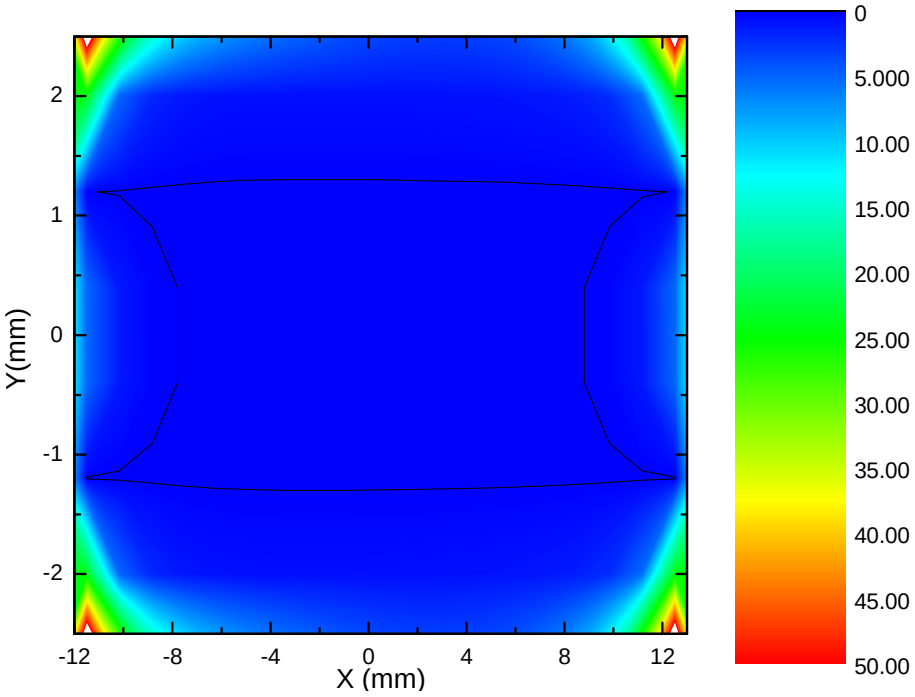

Fig. 4. 12. The distribution of the absolute value of relative changes of the absolute magnetic flux value. The origin of the coordinate system corresponds to the air gap centre. The hot colours correspond to big relative changes; the cold colours correspond to small relative changes. The whole colour scale corresponds to relative changes about 50 percent. The area surrounded by the black line has relative changes of the flux of less than 0.1%.

5. Conclusion.

The table shows the absolute value of the magnetic flux, in the centre of the air gap, in relation to its dependence on the excitation current.

0.001 A	$2.61*10^{-7}$ T
1 A	$2.61*10^{-4}$ T
10 A	$2.61*10^{-3}$ T
100 A	$2.61*10^{-2}$ T

The magnetic flux value in the centre of the gap is equal to $2.61 \cdot 10^{-3}$ T if the excitation current has a value of 10 A. For comparison, the magnetic flux value taken from a point in the free space which is located at the same distance from the excitation current, is equal to $1.7 \cdot 10^{-5}$ T. Thus, the gain caused by the presence of the yoke is about one hundred. Now comes the essential question: is this gain enough? Let's take the magnetic flux value for the excitation current that is equal to 10^{-3} A, and 100 A. The magnetic fields are correspondingly $2.61 \cdot 10^{-7}$ T and $2.61 \cdot 10^{-2}$ T. These two values define the dynamical range of the required magnetic field sensor. The AMR magnetic field sensors can measure the fields at the lower boundary but they are not able to measure the magnetic fields at the upper boundary. The Hall sensors are able to measure the magnetic fields at the upper boundary but will sense nothing at the lower boundary. The solution to this problem is the utilization of the magnetic field concentrator with a compensating winding, which will always hold the magnetic field in the magnetic yoke close to zero. Since the magnetic yoke field is held close to zero, one can use an AMR sensor. The sensitivity of the magnetic flux concentrator is fully defined by the magnetic field sensor sensitivity. The bandwidth of the magnetic field concentrator is defined by the bandwidth of the magnetic sensor and by the bandwidth of the feedback electronics.

A very important question about the measurements of such small currents is the influence of external magnetic fields. For example, the magnetic field of

the earth is about $5 \cdot 10^{-5}$ T. This value is comparable to the magnetic flux caused by a current of 0.1 A, and is a hundred times larger than the magnetic flux caused by a current of 1 mA. Thus, it is necessary to make a good magnetic shielding for the magnetic flux concentrator.

6. References.

[1] GSI Conceptual design report.

[2] K. Unser, IEEE Trans. Nucl. Sci., June 1961.

[3] K. Unser, IEEE Trans. Nucl. Sci., NS-28, p. 2344 (1981).

[4] Vacuumschmelze GmbH, Products Catalog.

[5] J.H. Coupland, T.C. Randle and M.J. Watson, *IEEE Trans. Magn*. **MAG-17**, 1851-1854 (1981)

[6] "*SYPRIS* Test&Measurement", Hall sensors datasheet. www.fwbell.com

[7] *SENTRON* AG, IMC-Hall sensors Datasheet.

[8] D.A. Thompson, L.T. Romankiw, A.F. Mayadas, *IEEE Trans. Magn*. **MAG-11**, 1039 (1975).

[9] Honeywell Sensor Products "1- and 2- Axis Magnetic Sensors", www.magneticsensors.com

[10] J. Daughton, J. Brown, R. Beech, A. Pohm, and W. Kude, *IEEE Trans.* **MAG-30**, 4608-4610 (1994).

[11] MAFIA v.4.024 Manual , April 2000.

Acknowledgements.

I would like to sincerely thank *Dr. Norbert Angert* for giving me the great opportunity to make my diploma thesis at GSI.

Without the help of *Dipl.-Phys. Andreas Peters* this work would not be imaginable. Thank you for discussions, advice and correction of this thesis.

I would like to express my gratitude to *Dipl.- Ing. Hansjörg Reeg* for the discussions and advice, to *Dipl.- Ing. Tino Giacomini*, *Dipl.- Ing. Tobias Hoffmann* for the help with a technical stuff.

Also I would thank all professors and senior lectors of the Department of Physics and Technology who have contributed to my education.

Mrs. Dennis Silberstein I would like thank for the time she have investigated to improve my English.